Non-target screening analysis reveals changes in the molecular composition of the Belukha Ice Core between the pre-industrial and industrial periods (1830-1980 CE)

François Burgay[1,2], Daniil Salionov[3], Thomas Singer[1,2,4], Anja Eichler[1,2], Sabina Brütsch[1], Theo Jenk[1,2], Saša Bjelić[3] & Margit Schwikowski[1,2,4]

[1] Laboratory of Environmental Chemistry (LUC), Paul Scherrer Institut, 5232 Villigen PSI, Switzerland

[2] Oeschger Centre for Climate Change Research, University of Bern, 3012, Bern, Switzerland

[3] Bioenergy and Catalysis Laboratory (LBK), Paul Scherrer Institut, 5232 Villigen PSI, Switzerland

[4] Department of Chemistry, Biochemistry and Pharmaceutical Sciences, University of Bern, 3012 Bern, Switzerland

Abstract

Ice cores are environmental archives that are used to reconstruct past changes in the atmospheric aerosol composition. Most ice-core studies have focused mainly on inorganic species and a few dozen organic molecules. However, organic compounds can account for up to 90% of the aerosol composition, meaning that only a fraction of the organic constituents has been studied, limiting our understanding of past atmospheric aerosol chemistry changes. Here, we present the first non-target screening ice-core record investigating the molecular composition of the Belukha ice core (Altai, Russian Federation) over the 1830-1980 CE period. We identified 491 molecules, mainly constituted by aliphatic secondary organic aerosol (SOA) species (e.g., dicarboxylic acids, ketoacids…) consisting of carbon, hydrogen, and oxygen atoms. Since 1955 CE, the ice-core molecular composition has changed with higher occurrence of nitrogen and sulfur-containing compounds, either associated to enhanced atmospheric reactions with anthropogenic-sourced NO_x and SO_2 or linked to direct emissions. During this period, we also observed an increase in the SOA oxygen-to-carbon ratio and average carbon oxidation state, suggesting an increase in the oxidative capacity of the atmosphere.

1. Introduction

Organic aerosol (OA) is a major component of atmospheric aerosol, accounting for 20-90% of the total aerosol mass (*1*). It can be classified into primary organic aerosol (POA), i.e. organic compounds emitted directly in the particulate form without undergoing any chemical reactions, and secondary organic aerosol (SOA), i.e. organic compounds that experience one or more chemical transformations in the gas phase, followed by condensation or nucleation (*2*). The main SOA precursors are volatile organic compounds (VOCs), which can be either anthropogenic (mainly composed of alkanes, aromatics and alkenes from fossil fuel combustion, transportation and industry) or biogenic (consisting mainly of isoprene and monoterpenes from terrestrial vegetation, grasslands, peatlands and forests) (*3, 4*). Once emitted into the atmosphere, VOCs are oxidized to SOA primarily by OH radicals, NO_x and O_3 (*5*). These reactions increase the polarity of the compounds, decrease their volatility and increase their hygroscopicity, favoring their condensation on available particles (*1*). Overall, these reactions

enhance OA capability to act as cloud condensation nuclei (*6*). Also considering its key role in absorbing and scattering the incoming solar radiation (*7*), OA is a pivotal player in the climate system and requires comprehensive chemical characterizations.

While the inorganic composition of atmospheric aerosol is well characterized, the molecular composition of the organic fraction is mainly uncertain and challenging to reveal due to the heterogeneity of SOA chemical properties and the large number of OA compounds (estimated to be between 10 000 and 100 000) (*8*). To overcome these difficulties several complementary mass spectrometry techniques exist. For example, Aerosol Mass Spectrometry (AMS) characterizes most of the organic aerosol mass and provides information on the functional groups, although it struggles to give the molecular formula of the compounds due to extensive molecular fragmentation (*9*). Due to the polar and water-soluble nature of most biogenic SOA, Liquid-Chromatography (LC) coupled with High-Resolution Mass Spectrometry (HRMS) equipped with soft ionization techniques (e.g. electrospray ionization, ESI) has emerged as a powerful technique to provide an accurate mass characterization of organic aerosol species, even though at the expense of a lower explanation of the total organic aerosol burden (*10*). The development of non-target screening (NTS) workflows that exploit the potential of high-resolution mass spectrometry, has unlocked the possibility of a detailed molecular characterization of OA (*11, 12*). While several NTS investigations of modern atmospheric aerosols exist (*13-15*), only a few NTS studies on the characterization of past OA through the analysis of ice cores has been reported in the literature (*16-19*). Furthermore, to our knowledge, there are no continuous NTS ice-core records aimed at achieving a comprehensive molecular characterization of OA over the past centuries. Indeed, the available long-term ice-core records are mainly focused either on inorganic species (*20-22*), or on the targeted characterization of biomass burning tracers (*23-27*), specific persistent organic pollutants (POPs) (*28-30*) and a few terrestrial and marine markers (*31, 32*), leaving a large organic fraction unknown and uncharacterized. The limited understanding of the chemical composition of OA acts as a barrier to comprehending SOA sources and atmospheric processing, thereby limiting our insights into past atmospheric OA composition and, consequently, on how it has changed during the Anthropocene.

To overcome this knowledge gap, we present the first NTS ice-core record from the Belukha glacier (Russian Federation), covering the period 1830-1980 CE. By applying a novel and sensitive methodology (*33*) we present an unprecedented continuous molecular characterization of the past atmospheric chemical composition in Central Asia. Through this investigation, we unravelled how natural and anthropogenic processes have affected the molecular composition of OA and we investigated how OA oxidation state has changed, providing a potential new tool for assessing past atmospheric oxidative capacities.

2. Material and Methods

2.1 Sampling site, sample processing and labware cleaning procedure

A 160-m long ice core was collected using an electromechanical drill at Belukha glacier (4062 m. a.s.l. - 49°48'26" N, 86°34'46" E, Figure S1) between 27 May and 10 June 2018. The core was drilled around 90 m NE of the 2001 drill site (*34*) and reached bedrock. After being collected, all cores were sealed in polyethylene (PE) tubes in the field and stored in insulated boxes. All samples were shipped frozen to Paul Scherrer Institut (Switzerland) and stored at -20°C until analyses. The samples analyzed in this study cover the time period 1830-1980 CE, i.e., from 26.55 to 74.11 meter-depth. Samples had a density ≥ 0.7 g cm^{-3}, thus minimizing risks for external contamination that can be present when more porous material, such as firn, is analyzed. More details on ice-core processing and the labware cleaning procedure are reported in SI.1.

2.2 Sample analysis

Details about the standards and solvents used for the extraction, analysis and identification are provided in Burgay et al., 2023. A brief explanation is provided in the SI 2.

2.3 Data processing

Data were pre-processed using Compound Discoverer 3.2 (ThermoFischer) and then threated for statistical analyses with MATLAB® (MathWorks).

Compound Discoverer settings: the settings used for Compound Discoverer are described in detail in the Supplementary Information of Burgay et al., 2023. Out of all the profiles identified, an additional filtering was applied: a) peak rating ≥ 7.0; b) *m/z* < 400; c) group CV ≤ 15%; d) formula is not blank, e) max intensity ≥ 5E6 and f) intensity threshold for the sample-to-blank ratio of 3.

Identifications: compounds were identified according to the Schymanski scale (*35*). To identify at level 2 the molecules found in the Belukha ice core, we used online spectral libraries (i.e. mzCloud and the NORMAN Mass Bank) for MS^2 spectra comparison (*36*). For level 1 identifications, an *in-house* database was used for MS^2 spectra and retention times (RTs) comparison between the suspects and the reference standards. The suspects were confirmed at level 1 when $\Delta RTs \leq 0.1$ min.

Statistical analyses: Hierarchical Cluster Analysis (HCA) was used to reduce the complexity of the dataset, to identify sample and molecular clusters and to prioritize molecular identifications. Initially, data were standardized based on *z*-transformation (`zscore` function), then clusterization was performed using the `clustergram` function with Euclidean as the metric for distance computation and the Ward method for creating the agglomerative hierarchical cluster tree. This setup was chosen among all the other possible methodologies since it provided an understandable and reproducible visualization of our dataset. The definition of the main clusters and sub-clusters was performed by drawing vertical lines that selected the clusters based on their similarities. To detect abrupt change points in the time series, the `findchangepts` function was used. Linear correlations were performed using the `corr` function and in case of missing data, linear interpolation was performed using the `interp1` function. To evaluate the significance of temporal trends, the `fitlm` function was used and the associated p-value was evaluated for significance. The statistical significance of the tests was set to 0.05. P-values are reported only when greater than 0.05.

126 *2.4 Ice core dating*

127 The ice was dated using $\delta^{18}O$ and NH_4^+ annual layer counting, constrained with the 1963 CE
128 nuclear fallout maximum detected by the ^3H peak, and with non-dust SO_4^{2-} peaks attributed to volcanic
129 eruptions (Katmai, 1912 CE; Krakatoa 1883 CE). The ice-core record presented in this work covers the
130 period 1830-1980. The dating uncertainty varies with proximity to the surface and the three reference
131 horizons (1963 CE, 1912 CE and 1883 CE), with at most ±5 years between 1883 and the surface and
132 ±10 years for the oldest part. Additional dating details are provided in (*37*).

133 **3. Results and Discussion**

134 4049 different features were identified in the Belukha ice core, out of those, 491 compounds were
135 filtered and used for environmental interpretations. The subset of filtered compounds correlates with
136 the unfiltered intensities (r = 0.96), indicating its representativeness (Figure S2). We examined how the
137 sum of the filtered compound intensities represented the variability observed in the dissolved organic
138 carbon (DOC) quantified by a photo-oxidation method (*38*). The DOC data from the Belukha ice core
139 are from (*37*) and they are used in this manuscript for comparison purposes only. We found a significant
140 correlation between the two variables (r = 0.590), indicating that the corrected intensities capture the
141 variability of the dissolved organic carbon content.

142 *3.1 General overview of the molecular fingerprint from the Belukha ice core*

143 Out of the 491 filtered molecules, 60% consist of carbon (C), hydrogen (H) and oxygen (O), 15%
144 also contain nitrogen (N), 8% also contain sulfur (S), 1% contained only C, H and S, and 16% contained
145 other heteroatoms (phosphorus, chlorine…) (Figure 1). In terms of average intensities calculated over
146 the 65 samples, CHO compounds account for up to 96% of the total intensity. This is explained both by
147 their greater occurrence and by the methodological setup, which was designed to enhance their
148 ionization efficiency. The remaining 4% is equally divided between CHNO and "other" molecules.
149 CHOS and CHNOS intensities have a marginal contribution. This can be explained by the fact that
150 these molecules were mainly present in the most recent part of the record (Figure 2) and by the
151 difficulties in analyzing S-containing compounds due to their high diversity (e.g., sulfides, thiophenes

or polyaromatic sulfur heterocycles). Indeed, the analysis of sulfur compounds generally requires optimized and dedicated analytical procedures and, in some cases, the use of specific ionization promoters or derivatization (*39*). Moreover, their analysis is typically performed in ESI(+) mode (*40*).

The Van Krevelen (Figure 1B) and Kroll (Figure 1C) diagrams are used to interpret HRMS results for a more comprehensive characterization. The Van Krevelen diagram shows that, on average, most of the compounds have a H/C ≥ 1.2 (n = 393), implying that the majority of the molecular entities in the Belukha ice core are aliphatic (Figure S3) (*41*). This is endorsed by the Double Bond Equivalent (defined as DBE = C – (H/2) + (N/2) +1, where C is the number of carbon atoms, H is the number of hydrogen atoms and halogen atoms, and N is the number of nitrogen atoms) distribution that shows most of the compounds having DBE ≤ 4 (n = 267) (Figure S4 – middle panel). Also, the O/C values for many compounds (n = 228) are on average ≥ 0.5, suggesting that a significant fraction of the observed molecules is composed by oxidation products of isoprene or monoterpenes (*42*) (Figure S3). We also noted compounds in the Van Krevelen diagram that line up along a line with a slope of -1 (H/C = 2, O/C = 2), which describes the progressive aerosol ageing of VOCs (e.g. monoterpenes, like α-pinene) after atmospheric oxidation (*42*).

The Kroll diagram plots the compounds according to their average carbon oxidation state (OS_C) and number of carbon atoms. OS_C is defined as $OS_C = 2\ O/C - H/C$ (*43*). This data representation is particularly useful for visualizing compounds according to their volatility. For example, low-volatility oxygenated organic aerosols (LV-OOA) have an OS_C between 0 and +0.9, while semi-volatile oxygenated organic aerosols (SV-OOA) have an OS_c between -0.5 and 0 (*44*). The Kroll diagram also provides preliminary information on the atmospheric oxidation pathways that monoterpenes or isoprene compounds undergo once emitted. For example, ozonolysis of monoterpenes results in an OS_C between -1.1 and -0.5, while the reaction of isoprene with OH radicals leads to OS_C between -0.8 and -0.2 (*43*). Overall, the Kroll diagram is an important tool for evaluating organic aerosol ageing that involves a progressive functionalization of the organic compounds (higher OS_C) along with their progressive fragmentation (lower number of carbon atoms). Tracking the temporal evolution of these parameters is fundamental to assess long-term changes in atmospheric oxidative capacities. According to the previous

definitions, in our record we observe the occurrence of both LV-OOA and SV-OOA, with most of the molecules being the result of oxidation of monoterpenes and isoprene compounds. The low occurrence of compounds with OS_C between -1.7 and -1.6 could either indicate the low abundance of hydrocarbon-like organic aerosol (HOA) in the samples or simply be a consequence of the analytical methodology, which is designed to detect water-soluble compounds (Figure S3).

3.2 Temporal profile

Compared to routine organic target analyses, the application of NTS allows for a wider and more comprehensive molecular characterization of OA. When applied to paleoenvironmental archives, NTS sheds light on changes in the aerosol molecular composition over the past centuries. In this study, we present the molecular composition changes observed at Belukha glacier over the last 150 years (1830-1980 CE). As shown in Figure 2, until the mid-1950s, CHO compounds (green), built up most of the total intensity (98%), with a residual contribution of CHNO compounds (violet, 1.5%) and others (light blue, 0.5%). On the contrary, between 1955 and 1980, the CHO share decreased to 88%, with an increasing contribution of CHNO (4%), CHNOS (yellow, 1%), CHOS (red, 0.1%) and others (7%). The higher occurrence of CHNO, CHNOS, CHOS and others coincides with the increasing trend in the ice concentration of nitrate and sulfate, which are proxies used to trace past NO_x and SO_2 emissions, respectively (*45, 46*). This suggests that the onset of industrialization in the FSU changed the molecular composition of atmospheric aerosols (Figure 3). Changes in the aerosol chemistry are also reflected by an increase in the weighted averaged DBE values that increased after 1955 CE from 2.39 ± 0.03 during the pre-industrial to 2.64 ± 0.07 (Figure S4 – upper panel) indicating that: a) unsaturated compounds with at least two double bonds, such as dicarboxylic acids, explained most of the aerosol intensity during the pre-industrial period and, b) that industrial aerosol is constituted by more unsaturated compounds, although organic compounds with a low unsaturation continues to build up a significant fraction of the overall intensity (Figure S4 – middle panels).

The reasons behind the observed change in the aerosol molecular composition can be linked to changes in the atmospheric oxidative pathways. For example, the intensity related to CHNO compounds

have increased 3-fold in the period 1955-1980, compared to 1830-1955 (Figure 2). The significant correlation between CHNO and NO_3^- (r = 0.569), suggests that these compounds are formed in the atmosphere after being oxidized by NO_x and that this reaction has been enhanced in the most recent period due to higher anthropogenic NO_x emissions. Indeed, while at low NO_x concentrations, the RO_2 radicals formed after the oxidation of the organic precursors (e.g. monoterpenes or isoprene compounds) react primarily with HO_2 to form organic hydroperoxides (ROOH), at high NO_x concentrations, RO_2 can also react with NO_2 to form organic nitrate (RO_2NO_2) (*5*). The DBE calculated for the CHNO compounds observed in the Belukha record is on average 6, supporting this hypothesis and suggesting the aromatic nature of these compounds. Similarly, a 16-fold increase in CHNOS and CHOS compound intensities was also observed in the period 1955-1980, compared to 1830-1955 (Figure 2), along with an increase in SO_4^{2-} concentration (r = 0.754; r = 0.747, respectively). The formation of organosulfates from the oxidation of biogenic VOCs occurs via several different pathways, including nucleophilic substitution of alcohols with sulfuric acid, sulfoxy-radical reactions and heterogeneous reactions with SO_2 (*3*). It has been estimated that organosulfate can make up to 30% of the organic aerosol mass fraction (*47*). However, in our record we observed a generally lower abundance of CHNOS and CHOS compounds than CHNO molecules, which is explained by the methodological setup, as discussed above. Although the emissions of NO_x and SO_2 have altered the atmospheric oxidative pathways, we cannot discard the hypothesis that some of these N- and S-containing compounds were emitted directly from pollution sources.

CHO compounds show a significant correlation with DOC (r = 0.613). The temporal profile of CHO shows a significant long-term decreasing trend from 1830 to 1923, followed by a mild, yet significant, increase over the last 60 years of the record (Figure 2). Their DBE ranges between 1 and 9, with an average value of 2.7, indicating that they are mainly aliphatic compounds. Since no CHO shows DBE = 0, neither aliphatic alcohols nor ethers were observed. Interestingly, CHO compounds do not correlate neither with NH_4^+ (r = 0.232, p-value = 0.06), which is a proxy for primary biogenic emissions (*48*), nor with $\delta^{18}O$ (r = -0.180, p-value = 0.152), which is a proxy for past temperature (*48*), indicating that they are mostly not related to primary emissions (see 3.3.2 for more details) but rather to

atmospheric oxidative processes. In this context, CHO compounds show a significant correlation with K^+ (r = 0.571), NO_3^- (r = 0.447) and SO_4^{2-} (r = 0.327) over the entire record, suggesting that they can be influenced both by the occurrence of wildfires in the Siberian boreal forest and by human activities, since K^+ and NO_3^- are related to both wildfires and anthropogenic emissions (*49*). Potassium is indeed a major electrolyte in plant cytoplasm and can be easily volatilized during combustion, while nitrate derives from the large nitrogen oxide emissions during forest fires that are then converted to HNO_3 and then detected as NO_3^- (*49, 50*). However, potassium may also have anthropogenic sources, primarily from fossil fuel combustion, similarly to NO_3^- and SO_4^{2-} (*49*). We disentangled the two contributions by evaluating K^+, NO_3^- and SO_4^{2-} correlations with CHO before 1923 (i.e., before the increasing trend was observed) and between 1923 and 1980. Statistical analysis showed similar significant correlations between CHO and K^+ and NO_3^- during the 1830-1923 period (r = 0.587 and r = 0.577, respectively), but not with SO_4^{2-} (r = 0.032, p-value = 0.851). During 1923-1980, correlations remain statistically significant with K^+ and NO_3^- (r = 0.562 and r = 0.525, respectively), but becomes statistically significant also with SO_4^{2-} (r = 0.560). Considering that SO_4^{2-} is not a proxy for biomass burning events during the pre-industrial period (*49*), we conclude that CHO intensities might have been mainly influenced by wildfires in the pre-industrial period and by anthropogenic emissions from the mid-1950s.

The wildfire contribution can be explained by the high emissions of LV-OOA and SV-OOA precursors (e.g. α- and β-pinene) that are observed during biomass burning events (*51*), promoted by locally high temperatures that enhance pinene emissions from the burning trees and their surroundings (*25*). In addition, forest fires are also a significant source of both OA (*52*) and oxidants (*53*), that can increase SOA yield and lead to high CHO intensities (*54*). It has also been reported that biomass burning is an important source of nitro-organic compounds (*55*). Looking at the record, we observe a significant long-term decreasing trend of CHNO compounds between 1830 and 1923, which is significantly correlated with CHO intensities (r = 0.470). Overall, the long-term decreasing trend of CHO observed from 1830 to 1923 together with the concurrent significant decreasing trends of CHNO, K^+ and NO_3^- can be associated with a decrease in forest fire activity (*49, 56*), which may have reduced the concentration of atmospheric oxidants (i.e. OH radicals, O_3 and NO_x), leading to a lower SOA yield

(*57*). Additional evidence comes from the observed decreasing trend in black carbon concentrations during the pre-industrial period (*37, 56*).

From 1923 to 1980, a slight increasing trend in CHO intensity was observed. Based on previous significant correlations between CHO and NO_3^-, K^+ and SO_4^-, we argue that the CHO trend may be influenced by progressively higher NO_x and SO_2 emissions due to the combustion of fossil fuels (e.g., coal) and the increase in road traffic. It has been demonstrated that anthropogenic pollutants control the formation of SOA. For example, satellite observations have shown that SOA formation is stronger in areas with high concentrations of NO_x and SO_2 (*58*). In addition, the presence of acidic aerosols, enhanced by the emissions of NO_x and SO_2 that are oxidized in the atmosphere to HNO_3 and H_2SO_4, acid-catalyzes SOA formation from isoprene or monoterpenes, which can proceed at a faster rate than under neutral conditions (*59*). It should also be considered that in addition to the formation of alkyl nitrate (CHNO) as shown above, the presence of NO_x during the industrial period also enhances the formation of CHO compounds, such as carboxylic acids (*60*) since NO_x can act as a source of OH radicals and O_3. All these contributions associated with anthropogenic emissions may have led to a moderate enhancement in CHO abundance during the last five decades of the record. However, it cannot be excluded that some of the identified CHO compounds have both natural and anthropogenic sources, as for example adipic acid and sebacic acid (*25*).

3.3 Hierarchical cluster analysis (HCA)

In previous paragraphs, we described the general features observed in our dataset. However, to improve the amount of information that can be obtained and to provide a more in-depth analysis on compound's temporal behavior, a Hierarchical cluster analysis (HCA) was performed. Interestingly, HCA performed on both the samples (x-axis in Figure S5) and the compounds (y-axis in Figure S5) led to the identification of two sample clusters and two molecular clusters.

The sample clusters were defined by the time period they covered. The first sample cluster (violet in Figure S5) was defined as the *"anthropogenic cluster"* because it covers the most recent part of the record, from 1955 to 1980 CE where sulfate and nitrate concentrations showed their stronger

285 increase. The second sample cluster (green in Figure S5) was defined as the *"natural cluster"*, because
286 it contains samples from the period 1830-1955 CE, i.e., when the anthropogenic contribution was small
287 or negligible, as also confirmed by the low nitrate and sulfate concentrations.

288 A similar classification was done for the molecular clusters. Two main molecular clusters were
289 identified (1 and 2), which were further subdivided into two sub-clusters (2A and 2B). Compounds
290 identified in cluster 1 (n = 214), were associated with anthropogenic emissions as they strongly correlate
291 with NO_3^- (r = 0.521), SO_4^{2-} (r = 0.537) and heavy metal profiles (Figure S6, Table S1). The compounds
292 identified in cluster 2 (n = 277) were associated with natural emissions as they were present throughout
293 the record and, based on the observed O/C and average carbon oxidation state, they include several
294 SOA species (Figure S7).

295 To visualize which molecules showed the largest increase from the pre-industrial to industrial
296 period, we used a volcano plot to highlight those compounds that showed the greatest change in intensity
297 between the industrial and pre-industrial periods (Figure S8). Based on HCA results, we use 1955 CE
298 as the year that defines both periods. Although not commonly used in environmental science, volcano
299 plots provide an effective way to visualize significant changes in the compound intensities and they can
300 be useful in prioritizing specific molecules of interest. More information related to volcano plots are
301 reported in SI3. As expected, the molecules showing the strongest and most significant change are those
302 belonging to cluster 1. A few compounds belonging to cluster 2A (n = 11) showed at least a 2-fold
303 increase in their intensity during the industrial period. Similarly, only a few species belonging to cluster
304 2B (n = 14) showed intensities at least 2-fold in the pre-industrial than during the industrial period.
305 Overall, the largest change in the molecular composition is ascribable to the anthropogenic entities,
306 while the natural compounds showed less variability, although present.

307 *3.3.1 Anthropogenic clusters*

308 Despite its location relatively far from industrialized contexts, Belukha ice core entrains in its
309 stratigraphy the effects of anthropogenic pollution as shown by the increasing trends of SO_4^{2-} and NO_3^-
310 , which are known proxies for fossil fuel combustion and traffic (Figure 2). Previous investigations

311 performed on a Belukha ice-core collected in 2001, also showed strong enhancement in heavy metal
312 concentrations (e.g. Cu, Zn, Sb and Cd) especially during the 1950s, due to the high number of Soviet
313 industries operating in the Altai region (*61*). Additionally, the use of tetraethyllead as an anti-knock
314 agent in fuels caused a remarkable increase (up to 300-fold compared to the pre-industrial period) in Pb
315 concentrations in the ice core during 1940-1970 (*62*).

316 In our investigation, we observed 214 compounds clustering in the *anthropogenic cluster*. From
317 a molecular point of view, 22% of the molecules presented C, H and O in their structure, 23%
318 compounds also presented N, 17% compounds also presented S, while 2% compounds presented only
319 C, H, O and S. 37% molecules showed other atomic combinations, including the occurrence of other
320 heteroatoms (e.g., phosphorus, chlorine). The high abundance of CHNO and CHNOS compounds
321 supports our interpretation of this molecular cluster as anthropogenic, since it may indicate stronger
322 atmospheric reactions with NO_x and SO_2, as discussed previously. This cluster is characterized by wide
323 weighted average O/C ratio (0.5 ± 0.3), OS_C (-0.6 ± 0.7), number of carbon atoms and number of oxygen
324 distribution that peaks at $n_O = 5$, but it extends until $n_O = 13$ (Figure S10). The generally high DBE
325 values (60% of compounds has DBE > 4) suggest the presence of aromatics.

326 The temporal profile of this cluster shows almost no variability until the 1940s, when most of
327 the compounds was absent, followed by a slight increase in the 1940s and a strong enhancement
328 between 1955 and 1980 (Figure S6). Looking at their molecular identities, the four compounds with the
329 highest area were, in descending order, $C_9H_{14}O_6$ (RT = 9.08 min), $C_8H_{16}O_6$ (RT = 6.32 min),
330 $C_7H_{16}N_2O_6P_2$ (RT = 6.84 min), $C_{23}H_{36}NOP$ (RT = 11.43 min), $C_9H_6N_4O_2$ (RT = 3.92 min).
331 Unfortunately, we could not increase our identification confidence level because we could not find any
332 matches between the acquired MS^2 spectra and the consulted online spectral libraries (mzCloud and the
333 NORMAN database). Nevertheless, our results show the occurrence of previously unknown substances
334 which may be related either to atmospheric processing or to their direct emission to the atmosphere
335 from the nearby industries (e.g. heavy machinery and chemical production (*61*)) (Table S1). More
336 efforts in the structural elucidation of these compounds are clearly needed and should be addressed in
337 future studies.

338 *3.3.2 Natural clusters*

339 Belukha mountain massif is in the Altai Mountains, which are surrounded by heterogeneous
340 climatic conditions: boreal forests in the north, desert, steppe and forest in the west, steppe and deserts
341 in the south and mountain larch forests, alpine and tundra-steppe vegetation in the east. This
342 heterogeneity is mirrored by the variety of biological proxies observed in the Belukha ice core such as
343 diatoms and pollens of coniferous, deciduous trees and herbs (*49, 63*), as well as by the occurrence of
344 biological inorganic (e.g. NH_4^+)(*48*) and organic (e.g. *n*-alkanes) tracers (*64*). However, a
345 comprehensive assessment of the molecular composition of natural compounds was missing.

346 In this study, we observed n = 277 different profiles (Cluster 2 or *natural cluster*) (Figure S5).
347 According to HCA, the *natural cluster* was further divided into two sub-clusters, namely 2A and 2B
348 consisting of 195 and 82 profiles, respectively (Figure S7). While the main cluster (cluster 2) does not
349 show a clear trend over the investigated period, the sub-clusters show distinct profiles. To understand
350 the reasons behind these different behaviors and their environmental implications, we describe the main
351 features associated with each sub-cluster.

352 **Cluster 2A.** This sub-cluster consists of 195 profiles (70% of cluster 2 profiles and 80% of cluster 2
353 total intensity): 91% CHO compounds, 6% CHNO, 0.5% CHNOS and 2% classified as "other" (Figure
354 S9). This sub-cluster correlates with DOC (r = 0.69). The average O/C weighted by compound
355 intensities is 0.70 ± 0.02, the weighted average carbon oxidation state is -0.13 ± 0.04 and the weighted
356 average number of carbon is 6. These values suggest that the compounds belonging to this sub-cluster
357 are SV-OOA and LV-OOA, likely products of atmospheric oxidation of isoprene molecules (*43*).
358 Looking at the number of oxygen distribution (Figure S11), most of the compounds have more than 3
359 oxygen atoms in their structure, with higher occurrences in the industrial period (60% of total
360 intensities) than in the pre-industrial period (52% of total intensities). According to the DBE distribution
361 (Figure S4), 70% of compounds belonging to this cluster have between 2 and 4 DBE, suggesting,
362 together with the observed oxygen atom distribution, the likely presence of dicarboxylic, tricarboxylic
363 acids and monounsaturated dicarboxylic acids. Their occurrence is corroborated by several homologues

corresponding to linear saturated dicarboxylic acids ($C_2H_2O_4(CH_2)_n$), linear unsaturated dicarboxylic acids ($C_2O_4(CH_2)_n$), linear hydroxycarboxylic acids ($CH_2O_3(CH_2)_n$), cyclic aliphatic dicarboxylic acids ($C_2O_4(CH_2)_n$), and by the identification at Level 1 and Level 2 of some of these acids. Succinic acid ($C_4H_6O_4$, RT = 3.68 min), glutaric acid ($C_5H_8O_5$, RT = 4.44 min), adipic acid ($C_6H_{10}O_4$, RT = 6.41 min), pimelic acid ($C_7H_{12}O_4$, RT = 8.17 min), sebacic acid ($C_{10}H_{18}O_4$, RT = 11.13 min), pinic acid ($C_9H_{14}O_4$, RT = 9.03 min) and p-hydroxybenzoic acid (PHBA, $C_7H_6O_3$, RT = 8.55 min) were identified at Level 1. At Level 2, we identified p-nitrophenol (4-PNP, $C_6H_5NO_3$, RT = 10.94 min, mzCloud Match = 92.7), p-hydroxybenzaldehyde (PHBAH, $C_7H_6O_2$, RT = 8.88 min, mzCloud match = 86.9), glycolic acid ($C_2H_4O_3$, RT = 7.52 min, mzCloud match = 92.9) and 2-3-dihydroxypropanoic acid ($C_3H_6O_4$, RT = 2.5 min, mzCloud match = 92.9). A more detailed list of the identified compounds is shown in Table S2, including those identified at Level 3.

While the overall temporal trend of cluster 2A shows little temporal variability, it hinders several different trends that we try to elucidate by looking at those of some of the identified compounds. For example, isomers of $C_7H_{10}O_5$ (RT = 5.02, 4.67 min), $C_6H_8O_4$ (RT = 8.86, 9.02, 8.987 min) and $C_5H_8O_4$ (RT = 9.46, 9.35 min) exhibit an abrupt increase since 1951 and, due to their statistically significant correlation in the industrial period with NO_3^- (r = 0.639), K^+ (r = 0.679) and SO_4^{2-} (r = 0.591), we hypothesize that this increase is likely induced by an increase in human activities that lead to an enhanced atmospheric chemical processing (*65*) (Figure S12). This enhancement, however, is modest in terms of intensity as shown by the volcano plot (Figure S8). The long term decreasing trend in the pre-industrial period of the identified biomass burning tracers (PHBA, PHBAH and 4-PNP), together with the similar trends that identified SOA tracers (succinic acid, glutaric acid, adipic acid, pimelic acid, sebacic acid and pinic acid) have, seem to endorse our initial interpretation that a lower occurrence in wildfires might have led to a decrease in the occurrence of highly oxygenated compounds as the ones present in this cluster, suggesting that wildfires themselves may be the main drivers for atmospheric ageing in a pre-industrial atmosphere (Figure S13). As an example, PHBA and succinic acid correlate well with BC (r = 0.60 and r = 0.60 respectively) and K^+ (r = 0.53 and r = 0.62, respectively) between 1830 and 1925 (i.e., before the rising trend in BC likely associated to the combustion of fossil fuels).

Cluster 2B. This sub-cluster consists of 82 profiles (30% of cluster 2 profiles and 20% of the total intensity). 85% is CHO molecules, 13% CHNO and 1% is classified as other (Figure S9). The sub-cluster is statistically insignificant correlated with DOC during both the industrial and pre-industrial periods (r = 0.415, and r = 0.275, respectively). Its temporal trend is decreasing throughout the record (Figure S7). Its average O/C, calculated as a weighted average over the whole record is 0.62 ± 0.02 and the average oxidation state of carbon is -0.41 ± 0.03 indicating that the molecules belonging to this cluster are less oxidized than cluster 2A. Also, the oxygen distribution (Figure S11), indicates a significantly lower abundance of compounds with a number of oxygen higher than 4. Contrarily to cluster 2A, most of the compounds belonging to cluster 2B have a DBE between 1 and 3 (Figure S4), while a higher number of molecules with a DBE between 6 and 8 was observed than in cluster 2A. This result suggests the presence of more mono and di-carboxylic acids as well as the greater occurrence of aromatics compounds. Within this sub-cluster we identified one molecule at level 1, namely levulinic acid ($C_5H_8O_3$, RT = 3.87 min) and one molecule at level 2, namely 2-hydroxycinnamic acid ($C_9H_8O_3$, RT = 9.20 min, mzCloud match = 83.5), which is a compound that is ubiquitous in plant materials (*66*). We also identified two compounds at level 3: $C_9H_8O_4$ (RT = 8.37 min) as either caffeic acid, p-hydroxyphenylpyruvic acid or 2-3-dihydro-1,4-benzodiozine-5-carboxylic acid, and $C_8H_8O_3$ (RT = 9.83 min) as either 3-methylsalicylic acid, 4-hydroxy-2-methylbenzoic acid or p-hydroxyphenylacetic acid. Their molecular formula suggests that they are lignin degradation products and likely originate from biomass burning events (*67*). One main homologue series was identified and consists of ketoacids with general formula $C_3H_4O_3(CH_2)_n$ where n_C = 5 (levulinic acid), 6, 7, 8, 9 and 10. Ketoacids are thought to be intermediate in the photochemical oxidation of natural compounds (*68*) and they can be associated to biomass burning (*69*), so their decreasing trend in the pre-industrial period may be associated with a decreasing fire frequency, consistent with the correlation with K^+ (r = 0.58) and similar to what observed in cluster 2A. The decreasing trend observed in the industrial period can be related to: 1) lower hardwood combustion, as suggested by the presence of caffeic acid, or 2) a progressively more oxidizing atmosphere, meaning that that the oxidation products observed in this cluster (SV-OOA) are decreasing in favor of more oxidized compounds (LV-OOA), found in cluster 2A (Figure S14).

3.4 Environmental implications

In previous paragraphs, we have explored and described the molecular composition of each cluster and sub-cluster, trying to understand their environmental significance and explain the underlying mechanisms of SOA formation in the atmosphere. However, in the absence of reference standards, this remains a challenge due to our partial knowledge of the identity of the molecules, which was possible only up to level 4 for most of the compounds. Nevertheless, since NTS allows the identification of an unprecedented number of molecules from a single ice-core sample, in this study, we evaluated how the relative abundance of the compounds belonging to cluster 2 has changed before and during industrialization to assess any changes in the overall oxidation of the molecules.

Atmospheric oxidative capacity is defined as the global mean tropospheric abundance of the hydroxyl radical, which along with nitrate radicals, ozone and hydrogen peroxide, plays a major role in the oxidation of trace gases and organic compounds in the atmosphere (*70*). Anthropogenic activities affect the $^{\bullet}OH$ concentration in the atmosphere through the emission of NO_x, which favors the production of tropospheric O_3 and OH radicals. Conversely, CO, volatile organic compounds (VOCs) and CH_4 act as a sink for OH radicals, meaning that a fundamental understanding of how much the oxidative capacity of the atmosphere has changed from the pre-industrial to the industrial periods is not trivial. As an example, a large inter-model comparison shows that the magnitude of OH radicals change from pre-industrial to present day ranges from a decrease of 12.7% to an increase of 15.6%, with large regional differences (*71, 72*). This large uncertainty is also related to the difficulties in reconstructing the past atmospheric oxidative capacity from paleoenvironmental archives, such as ice cores. Attempts have been made by analyzing hydrogen peroxide (*73*) or the formaldehyde-to-methane ratio (*74*), with results that are highly debated (*70*). In this study, we propose an alternative approach based on the evaluation of the weighted average O/C and average oxidation carbon state after a comprehensive NTS study of the molecular composition of the Belukha ice core. The underlying assumption of our interpretation is that OH radicals react with VOCs and that higher carbon oxidation state and O/C correspond to higher atmospheric OH radical concentrations in the atmosphere (*1*).

In the Belukha ice-core record, we observe relatively constant O/C and OS_C values before 1952 (0.68 ± 0.01 and -0.20 ± 0.03, respectively). In 1952, an abrupt change point was identified in the time series of both variables, indicating a slight, but still significant, increase up to 0.70 ± 0.02 and -0.15 ± 0.04, respectively (Figure 4). Interestingly, this increase corresponds to the period when nitrate and sulphate shows remarkable increases, although their abrupt changes were not recorded until 1963, together with heavy metals (Table S1). This evidence led us to hypothesize that anthropogenic emissions have caused an increase in atmospheric oxidants that lead to the formation of more oxidized compounds, as shown both by the increase in the O/C ratio and in the increase in the relative intensities of cluster 2A, which is constituted by highly oxygenated compounds. This hypothesis is supported by modelling studies that highlighted an increase in OH radical concentrations in the industrial period compared to the pre-industrial one, from the source areas of Belukha (*71*). If verified, the higher $^{\cdot}OH$ concentration in the Siberian Altai region during the Anthropocene may have profound implications for Earth's radiative forcing. The effects are twofold: a) higher OH radical concentrations imply consequences on the atmospheric lifetime of methane, potentially shortening it compared to pre-industrial times (*72*); b) heightened polarity of compounds infers an increase in their hygroscopicity, i.e., their tendency to absorb water vapor and consequently act as cloud condensation nuclei.

4. Conclusions

In this manuscript, we have delved into the potentialities of utilizing NTS in ice-core analyses. The NTS analysis of the Belukha ice core unveiled the presence of 491 distinct molecules, primarily aliphatic compounds with carboxylic groups, as indicated by their molecular composition, oxygen distribution, and DBE values. The application of HCA simplified the interpretation of the dataset revealing two main clusters: an anthropogenic cluster spanning 1955-1980 CE, and a natural cluster spanning 1830-1955 CE. The anthropogenic cluster predominantly includes CHNO, CHNOS, and CHOS compounds, whose intensities strongly correlate with heavy metals, SO_4^{2-} and NO_3^-, i.e., proxies for environmental pollution. Given their occurrence at relatively low sample enrichment factors, we hypothesize that their source should be located close to the Belukha glacier, for example, in the Fergana and/or the Kuznetsk regions. The natural cluster primarily consists of SOA compounds composed by

carbon, hydrogen and oxygen atoms. Given their positive correlations with K^+, NO_3^- and BC in the pre-industrial period, we hypothesize that their occurrence is mainly influenced by wildfires. During the industrial period, a higher presence of more oxygenated compounds is observed that, together with increased O/C and OS_C values, may imply an enhanced atmospheric oxidative capacity.

While further validation through additional evidence and modeling studies is warranted, our findings introduce a promising avenue for future paleo-environmental investigations, offering a new potential tool to reconstruct past atmospheric oxidative capacity from mid-latitude ice cores.

Figures and Tables

Figure 1 – Panel A): *mass-to-charge* ratio against retention time for the 491 profiles identified after filtering (see main text for more details). Panel B): Van-Krevelen diagram. Panel C): Kroll diagram. Colors refer to the molecular class (green: CHO, violet: CHNO, yellow: CHNOS, red: CHOS and light blue: other). The size of the circles is proportional to the average intensity of the specific molecules over the 65 samples.

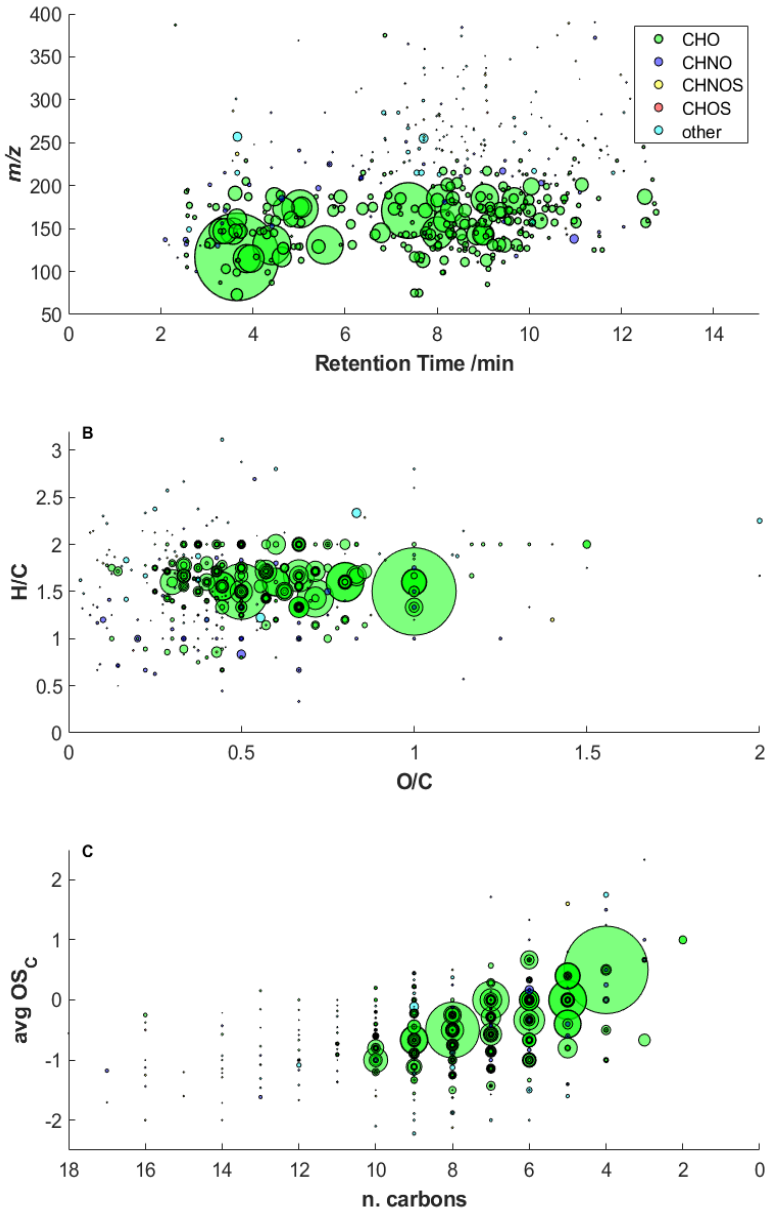

Figure 2 – Temporal profile of the different compounds identified in the Belukha ice core from 1830 to 1980, together with their distinct trends according to their molecular composition. CHO compounds are in green, CHNO compounds are in violent, CHNOS in yellow, CHOS in red and other compounds in light blue. The profile of nitrate and sulphate are also reported (black lines).

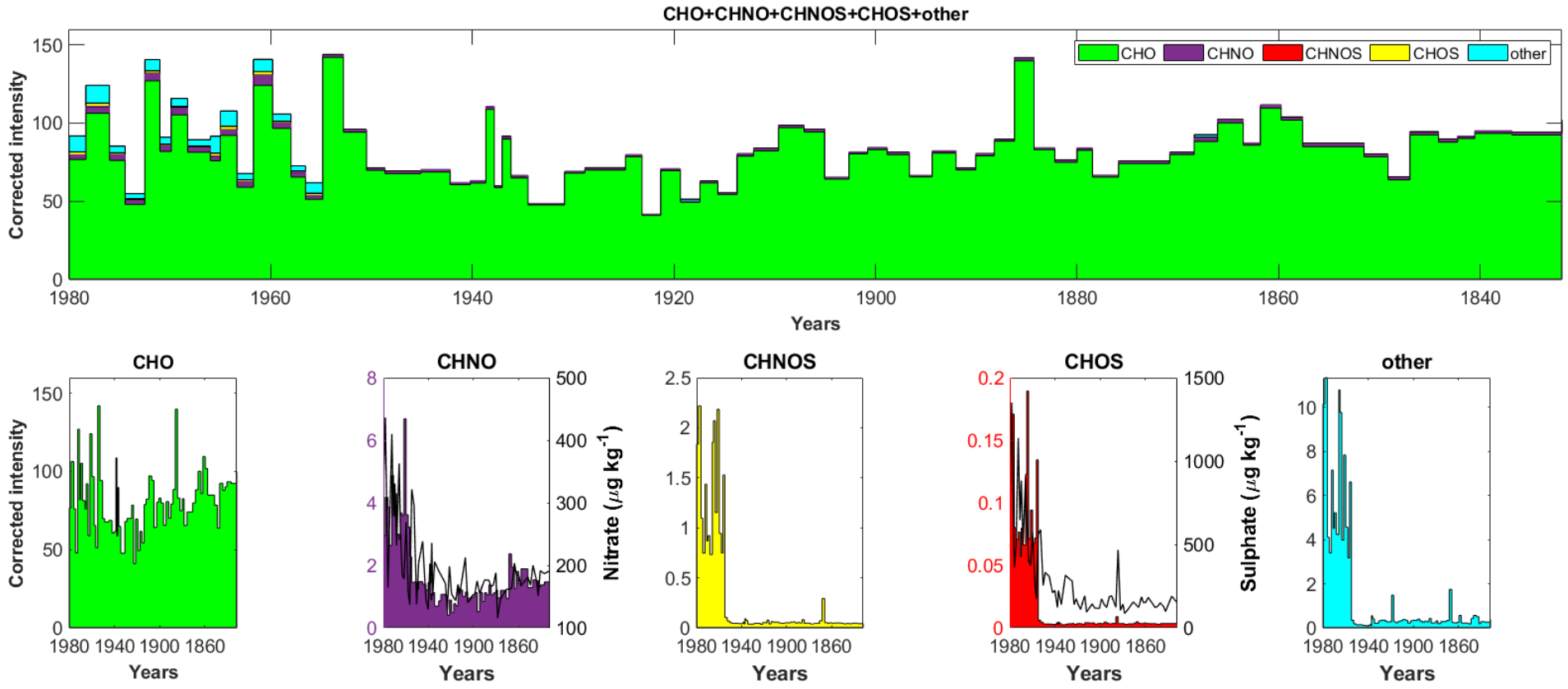

Figure 3 – Comparison between two samples, one referring to 1980 CE (industrial period) and the other referring to 1830 CE (pre-industrial period). Each dot represents a molecule, whose color defines its atomic composition, and the size defines its intensity. It is clearly visible how in the industrial sample, new molecular entities emerged, mainly constituted by nitrogen, sulfur, and other heteroatoms.

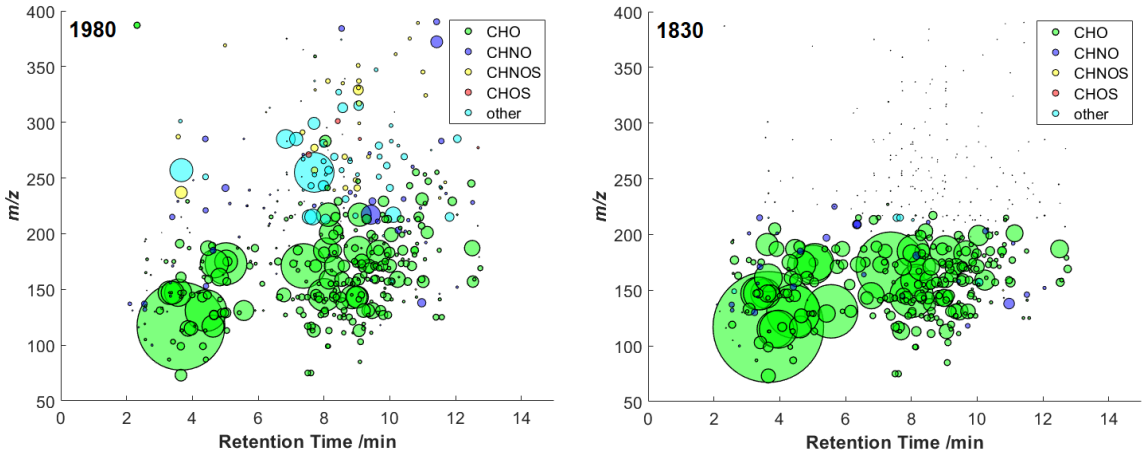

Figure 4 – The oxygen-to-carbon ratio and the average carbon oxidation state temporal profiles are reported together with the nitrate profile (orange line). The dotted green vertical lines represent the abrupt change point observed in 1952 for both profiles, suggesting an increase in atmospheric oxidative capacities due to anthropogenic pollution.

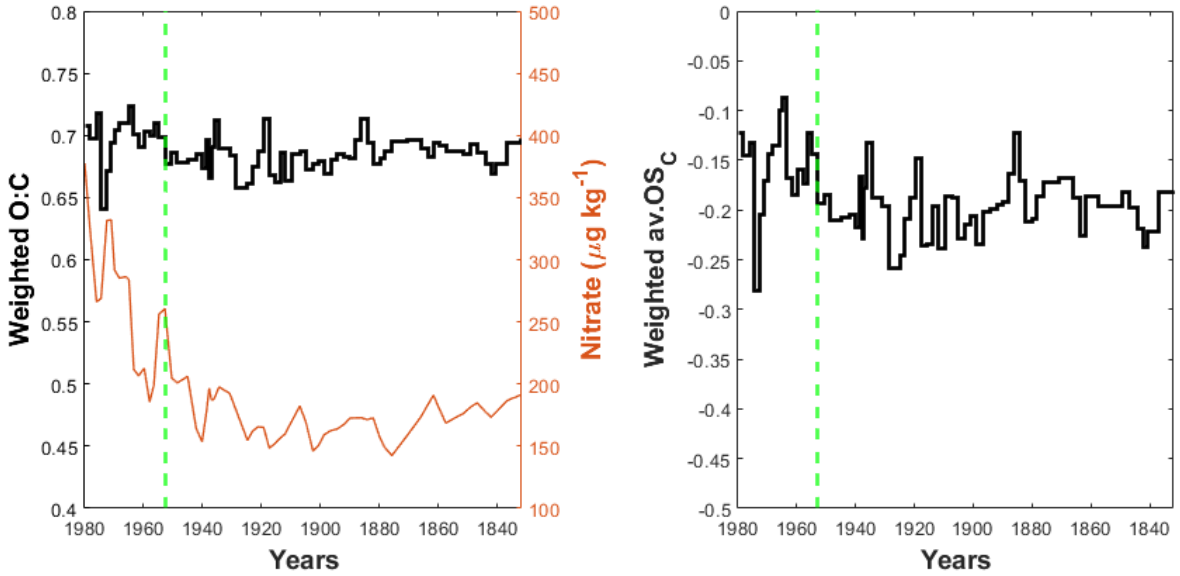

REFERENCES

1. J. L. Jimenez *et al.*, Evolution of organic aerosols in the atmosphere. *Science* **326**, 1525-1529 (2009).
2. L. Qi *et al.*, A 1-year characterization of organic aerosol composition and sources using an extractive electrospray ionization time-of-flight mass spectrometer (EESI-TOF). *Atmospheric Chemistry and Physics* **20**, 7875-7893 (2020).
3. D. Srivastava, T. V. Vu, S. Tong, Z. Shi, R. M. Harrison, Formation of secondary organic aerosols from anthropogenic precursors in laboratory studies. *npj Climate and Atmospheric Science* **5**, 22 (2022).
4. J. Cao, S. Situ, Y. Hao, S. Xie, L. Li, Enhanced summertime ozone and SOA from biogenic volatile organic compound (BVOC) emissions due to vegetation biomass variability during 1981–2018 in China. *Atmospheric Chemistry and Physics* **22**, 2351-2364 (2022).
5. M. Hallquist *et al.*, The formation, properties and impact of secondary organic aerosol: current and emerging issues. *Atmospheric chemistry and physics* **9**, 5155-5236 (2009).
6. G. McFiggans *et al.*, The effect of physical and chemical aerosol properties on warm cloud droplet activation. *Atmospheric Chemistry and Physics* **6**, 2593-2649 (2006).
7. J. H. Seinfeld *et al.*, Improving our fundamental understanding of the role of aerosol− cloud interactions in the climate system. *Proceedings of the National Academy of Sciences* **113**, 5781-5790 (2016).
8. A. H. Goldstein, I. E. Galbally. (ACS Publications, 2007).
9. V. Lanz *et al.*, Characterization of aerosol chemical composition with aerosol mass spectrometry in Central Europe: an overview. *Atmospheric Chemistry and Physics* **10**, 10453-10471 (2010).
10. J. Ma *et al.*, Nontarget screening exhibits a seasonal cycle of PM2. 5 organic aerosol composition in Beijing. *Environmental Science & Technology*, (2022).
11. C. Giorio *et al.*, Direct target and non-target analysis of urban aerosol sample extracts using atmospheric pressure photoionisation high-resolution mass spectrometry. *Chemosphere* **224**, 786-795 (2019).
12. H. Lamkaddam *et al.*, Large contribution to secondary organic aerosol from isoprene cloud chemistry. *Science advances* **7**, eabe2952 (2021).
13. K. Wang *et al.*, Urban organic aerosol composition in eastern China differs from north to south: molecular insight from a liquid chromatography–mass spectrometry (Orbitrap) study. *Atmospheric Chemistry and Physics* **21**, 9089-9104 (2021).
14. S. A. Nizkorodov, J. Laskin, A. Laskin, Molecular chemistry of organic aerosols through the application of high resolution mass spectrometry. *Physical Chemistry Chemical Physics* **13**, 3612-3629 (2011).
15. K. R. Daellenbach *et al.*, Impact of anthropogenic and biogenic sources on the seasonal variation in the molecular composition of urban organic aerosols: a field and laboratory study using ultra-high-resolution mass spectrometry. *Atmospheric Chemistry and Physics* **19**, 5973-5991 (2019).
16. A. L. Vogel *et al.*, A comprehensive nontarget analysis for the molecular reconstruction of organic aerosol composition from glacier ice cores. *Environmental Science & Technology* **53**, 12565-12575 (2019).
17. J. Xu *et al.*, High-resolution mass spectrometric characterization of dissolved organic matter from warm and cold periods in the NEEM ice core. *Sciences in Cold and Arid Regions* **10**, 38-46 (2018).
18. A. M. Grannas, W. C. Hockaday, P. G. Hatcher, L. G. Thompson, E. Mosley-Thompson, New revelations on the nature of organic matter in ice cores. *Journal of Geophysical Research: Atmospheres* **111**, (2006).

19. R. Zangrando *et al.*, Dissolved organic matter in the deep TALDICE ice core: A nano-UPLC-nano-ESI-HRMS method. *Science of the Total Environment* **700**, 134432 (2020).
20. F. Burgay *et al.*, Atmospheric Fe supply has a negligible role in promoting marine productivity in the Glacial North Pacific Ocean. *Clim. Past Discuss.* **2020**, 1-21 (2020).
21. S. Schüpbach *et al.*, Greenland records of aerosol source and atmospheric lifetime changes from the Eemian to the Holocene. *Nature communications* **9**, 1-10 (2018).
22. E. Wolff *et al.*, Changes in environment over the last 800,000 years from chemical analysis of the EPICA Dome C ice core. *Quaternary Science Reviews* **29**, 285-295 (2010).
23. D. Osmont, M. Sigl, A. Eichler, T. M. Jenk, M. Schwikowski, A Holocene black carbon ice-core record of biomass burning in the Amazon Basin from Illimani, Bolivia. *Climate of the Past* **15**, 579-592 (2019).
24. M. M. Grieman, M. Aydin, E. Isaksson, M. Schwikowski, E. S. Saltzman, Aromatic acids in an Arctic ice core from Svalbard: a proxy record of biomass burning. *Climate of the Past* **14**, 637-651 (2018).
25. C. Müller-Tautges *et al.*, Historic records of organic compounds from a high Alpine glacier: influences of biomass burning, anthropogenic emissions, and dust transport. *Atmospheric chemistry and physics* **16**, 1029-1043 (2016).
26. M. Rubino, A. D'Onofrio, O. Seki, J. A. Bendle, Ice-core records of biomass burning. *The Anthropocene Review* **3**, 140-162 (2016).
27. P. Zennaro *et al.*, Fire in ice: two millennia of boreal forest fire history from the Greenland NEEM ice core. *Climate of the Past* **10**, 1905-1924 (2014).
28. P. A. Pavlova *et al.*, Release of PCBs from Silvretta glacier (Switzerland) investigated in lake sediments and meltwater. *Environmental science and pollution research* **23**, 10308-10316 (2016).
29. M. Vecchiato *et al.*, The Great Acceleration of fragrances and PAHs archived in an ice core from Elbrus, Caucasus. *Scientific reports* **10**, 1-10 (2020).
30. W. F. Hartz *et al.*, Levels and distribution profiles of Per-and Polyfluoroalkyl Substances (PFAS) in a high Arctic Svalbard ice core. *Science of the Total Environment* **871**, 161830 (2023).
31. A. C. King *et al.*, Direct injection liquid chromatography high-resolution mass spectrometry for determination of primary and secondary terrestrial and marine biomarkers in ice cores. *Analytical chemistry* **91**, 5051-5057 (2019).
32. A. C. King *et al.*, A new method for the determination of primary and secondary terrestrial and marine biomarkers in ice cores using liquid chromatography high-resolution mass spectrometry. *Talanta* **194**, 233-242 (2019).
33. F. Burgay *et al.*, Hybrid Targeted/Untargeted Screening Method for the Determination of Wildfire and Water-Soluble Organic Tracers in Ice Cores and Snow. *Analytical chemistry*, (2023).
34. S. Olivier *et al.*, Glaciochemical investigation of an ice core from Belukha glacier, Siberian Altai. *Geophysical Research Letters* **30**, (2003).
35. E. L. Schymanski *et al.*, Identifying small molecules via high resolution mass spectrometry: communicating confidence. (2014).
36. V. Dulio *et al.*, Emerging pollutants in the EU: 10 years of NORMAN in support of environmental policies and regulations. *Environmental Sciences Europe* **30**, 1-13 (2018).
37. T. Singer, University of Bern, (2023).
38. L. Fang *et al.*, Extraction of dissolved organic carbon from glacier ice for radiocarbon analysis. *Radiocarbon* **61**, 681-694 (2019).
39. H. Müller, J. T. Andersson, W. Schrader, Characterization of high-molecular-weight sulfur-containing aromatics in vacuum residues using Fourier transform ion cyclotron resonance mass spectrometry. *Analytical Chemistry* **77**, 2536-2543 (2005).

40. X. Chen *et al.*, Direct sulfur-containing compounds analysis in petroleum via (+) ESI FT-ICR MS using HBF4 as ionization promoter. *Fuel* **278**, 118334 (2020).
41. F. Ungeheuer, D. van Pinxteren, A. L. Vogel, Identification and source attribution of organic compounds in ultrafine particles near Frankfurt International Airport. *Atmospheric Chemistry and Physics* **21**, 3763-3775 (2021).
42. C. Heald *et al.*, A simplified description of the evolution of organic aerosol composition in the atmosphere. *Geophysical Research Letters* **37**, (2010).
43. J. H. Kroll *et al.*, Carbon oxidation state as a metric for describing the chemistry of atmospheric organic aerosol. *Nature chemistry* **3**, 133-139 (2011).
44. M. Sueur *et al.*, PyC2MC: an open-source software solution for visualization and treatment of high-resolution mass spectrometry data. *Journal of the American Society for Mass Spectrometry* **34**, 617-626 (2023).
45. D. Samyn, C. P. Vega, H. Motoyama, V. A. Pohjola, Nitrate and sulfate anthropogenic trends in the 20th century from five Svalbard ice cores. *Arctic, Antarctic, and Alpine Research* **44**, 490-499 (2012).
46. M. Schwikowski, A. Döscher, H. Gäggeler, U. Schotterer, Anthropogenic versus natural sources of atmospheric sulphate from an Alpine ice core. *Tellus B: Chemical and Physical Meteorology* **51**, 938-951 (1999).
47. J. D. Surratt *et al.*, Organosulfate formation in biogenic secondary organic aerosol. *The Journal of Physical Chemistry A* **112**, 8345-8378 (2008).
48. A. Eichler, S. Brütsch, S. Olivier, T. Papina, M. Schwikowski, A 750 year ice core record of past biogenic emissions from Siberian boreal forests. *Geophysical research letters* **36**, (2009).
49. A. Eichler *et al.*, An ice-core based history of Siberian forest fires since AD 1250. *Quaternary Science Reviews* **30**, 1027-1034 (2011).
50. M. Legrand *et al.*, Boreal fire records in Northern Hemisphere ice cores: a review. *Climate of the Past* **12**, 2033-2059 (2016).
51. I. J. Simpson *et al.*, Boreal forest fire emissions in fresh Canadian smoke plumes: C 1-C 10 volatile organic compounds (VOCs), CO 2, CO, NO 2, NO, HCN and CH 3 CN. *Atmospheric Chemistry and Physics* **11**, 6445-6463 (2011).
52. C. N. Vasilakopoulou *et al.*, Rapid transformation of wildfire emissions to harmful background aerosol. *npj Climate and Atmospheric Science* **6**, 218 (2023).
53. K. Pan, I. C. Faloona, The impacts of wildfires on ozone production and boundary layer dynamics in California's Central Valley. *Atmospheric Chemistry and Physics* **22**, 9681-9702 (2022).
54. I. Konovalov *et al.*, The role of semi-volatile organic compounds in the mesoscale evolution of biomass burning aerosol: a modeling case study of the 2010 mega-fire event in Russia. *Atmospheric Chemistry and Physics* **15**, 13269-13297 (2015).
55. A. Kahnt *et al.*, One-year study of nitro-organic compounds and their relation to wood burning in PM10 aerosol from a rural site in Belgium. *Atmospheric Environment* **81**, 561-568 (2013).
56. S. Eckhardt *et al.*, Revised historical Northern Hemisphere black carbon emissions based on inverse modeling of ice core records. *Nature Communications* **14**, 271 (2023).
57. Y. He *et al.*, Formation of secondary organic aerosol from wildfire emissions enhanced by long-time ageing. *Nature Geoscience*, (2024).
58. A. H. Goldstein, C. D. Koven, C. L. Heald, I. Y. Fung, Biogenic carbon and anthropogenic pollutants combine to form a cooling haze over the southeastern United States. *Proceedings of the National Academy of Sciences* **106**, 8835-8840 (2009).
59. J. H. Kroll, J. H. Seinfeld, Chemistry of secondary organic aerosol: Formation and evolution of low-volatility organics in the atmosphere. *Atmospheric Environment* **42**, 3593-3624 (2008).

60. Y. Zhang, M. Cheng, J. Gao, J. Li, Review of the influencing factors of secondary organic aerosol formation and aging mechanism based on photochemical smog chamber simulation methods. *Journal of Environmental Sciences* **123**, 545-559 (2023).
61. A. Eichler *et al.*, Ice-core based assessment of historical anthropogenic heavy metal (Cd, Cu, Sb, Zn) emissions in the Soviet Union. *Environmental science & technology* **48**, 2635-2642 (2014).
62. A. Eichler *et al.*, Three centuries of Eastern European and Altai lead emissions recorded in a Belukha ice core. *Environmental science & technology* **46**, 4323-4330 (2012).
63. T. Papina *et al.*, Biological proxies recorded in a Belukha ice core, Russian Altai. *Climate of the Past* **9**, 2399-2411 (2013).
64. T. Miyake *et al.*, Concentrations and source variations of n-alkanes in a 21 m ice core and snow samples at Belukha glacier, Russian Altai mountains. *Annals of Glaciology* **43**, 142-147 (2006).
65. S. Kundu *et al.*, A sub-decadal trend in diacids in atmospheric aerosols in eastern Asia. *Atmospheric Chemistry and Physics* **16**, 585-596 (2016).
66. B. Krimmel, F. Swoboda, S. Solar, G. Reznicek, OH-radical induced degradation of hydroxybenzoic-and hydroxycinnamic acids and formation of aromatic products—A gamma radiolysis study. *Radiation Physics and Chemistry* **79**, 1247-1254 (2010).
67. W. Li *et al.*, Molecular characterization of biomass burning tracer compounds in fine particles in Nanjing, China. *Atmospheric Environment* **240**, 117837 (2020).
68. K. Kawamura, H. Kasukabe, L. A. Barrie, Source and reaction pathways of dicarboxylic acids, ketoacids and dicarbonyls in arctic aerosols: One year of observations. *Atmospheric Environment* **30**, 1709-1722 (1996).
69. S. Mkoma, K. Kawamura, Molecular composition of dicarboxylic acids, ketocarboxylic acids, α-dicarbonyls and fatty acids in atmospheric aerosols from Tanzania, East Africa during wet and dry seasons. *Atmospheric Chemistry and Physics* **13**, 2235-2251 (2013).
70. B. Alexander, L. J. Mickley, Paleo-perspectives on potential future changes in the oxidative capacity of the atmosphere due to climate change and anthropogenic emissions. *Current Pollution Reports* **1**, 57-69 (2015).
71. L. Murray *et al.*, Factors controlling variability in the oxidative capacity of the troposphere since the Last Glacial Maximum. *Atmospheric Chemistry and Physics* **14**, 3589-3622 (2014).
72. V. Naik *et al.*, Preindustrial to present-day changes in tropospheric hydroxyl radical and methane lifetime from the Atmospheric Chemistry and Climate Model Intercomparison Project (ACCMIP). *Atmospheric Chemistry and Physics* **13**, 5277-5298 (2013).
73. A. Sigg, A. Neftel, Evidence for a 50% increase in H202 over the past 200 years from a Greenland ice core. *Nature* **351**, 557-559 (1991).
74. T. Staffelbach, A. Neftel, B. Stauffer, D. Jacob, A record of the atmospheric methane sink from formaldehyde in polar ice cores. *Nature* **349**, 603-605 (1991).

Non-target screening analysis reveals changes in the molecular composition of the Belukha Ice Core between the pre-industrial and industrial periods (1830-1980 CE)

SUPPLEMENTARY INFORMATION

François Burgay[1,2], Daniil Salionov[3], Thomas Singer[1,2,4], Anja Eichler[1,2], Sabina Brütsch[1], Theo Jenk[1,2], Saša Bjelić[3] & Margit Schwikowski[1,2,4]

[1] Laboratory of Environmental Chemistry (LUC), Paul Scherrer Institut, 5232 Villigen PSI, Switzerland

[2] Oeschger Centre for Climate Change Research, University of Bern, 3012, Bern, Switzerland

[3] Bioenergy and Catalysis Laboratory (LBK), Paul Scherrer Institut, 5232 Villigen PSI, Switzerland

[4] Department of Chemistry, Biochemistry and Pharmaceutical Sciences, University of Bern, 3012 Bern, Switzerland

SI 1 Sample processing and labware cleaning procedure

After being shipped to Paul Scherrer Institut (Switzerland), the ice cores were cut. Ice cutting was performed in a cold room at -20°C using a modified band saw with a stainless steel blade and a polytetrafluoroethylene (PTFE) tabletop. All surfaces in contact with the core (i.e. the bandsaw, the tabletop and the saw guide) were cleaned at the beginning of the cutting day and after each core with acetone (Reag. Ph. Eur., VWR Chemicals). The operators wore gloves covered with PE gloves that were changed after each core to avoid sample cross-contamination. To avoid any contamination from the ice-core drilling operations as well as from the ice core handling and storage, the outermost part (≈1 cm) of each ice-core section was removed. The decontaminated inner ice-core parts were used for organic analyses. A section of 2.4 x 2.5 x 50 cm was cut for organic analyses (including particulate and dissolved organic carbon analysis and their radiocarbon fraction). A total number of 65 samples were collected for the NTS analyses of organic tracers from between 26.55- and 74.11-meters depth. The ice samples for organic analyses were stored in pre-cleaned PE jars (see §2.2 for details about the labware cleaning procedure) and they were kept frozen at -20°C until solid phase extraction (SPE).

To avoid any contamination, all the containers used in this investigation were carefully cleaned and decontaminated. In particular, the cut ice-core sections for organic analyses were stored in 2 L PE jars that were previously filled with ultrapure water (UPW) for at least 24 hours, then rinsed with UPW and refilled with UPW for an additional 24 hours. This procedure was repeated five times for each PE jar. The jars were then dried overnight under a Class-1000 laminar flow hood. The 50 mL glass vials (Infochroma, AG) used to store the molten core samples before solid-phase extraction, the 1.5 mL MS-vials (BG Analytics) used for organic analyses and the 1.5 mL tubes (Eppendorf) used for the standard solution preparation were cleaned as described in Burgay et al., 2023. Filters (PALLFLEX, Tissuquartz filters 2500QAT-UP, diameter of 47 mm) used for collecting the particulate organic carbon and to filter the samples for the NTS analyses were baked at 800°C for 5 hours.

For major ions analyses, the 50 mL PE tubes were cleaned as the PE jars, but they were dried into an oven at 65°C overnight.

Figure S1 – Panel A): The location of Belukha glacier is highlighted with a red triangle. Panel B): the detailed location of the drilling is reported where *2018 SNF* is the core investigated in this study, while *Drill site 2001* refers to the location of the ice core collected in 2001.

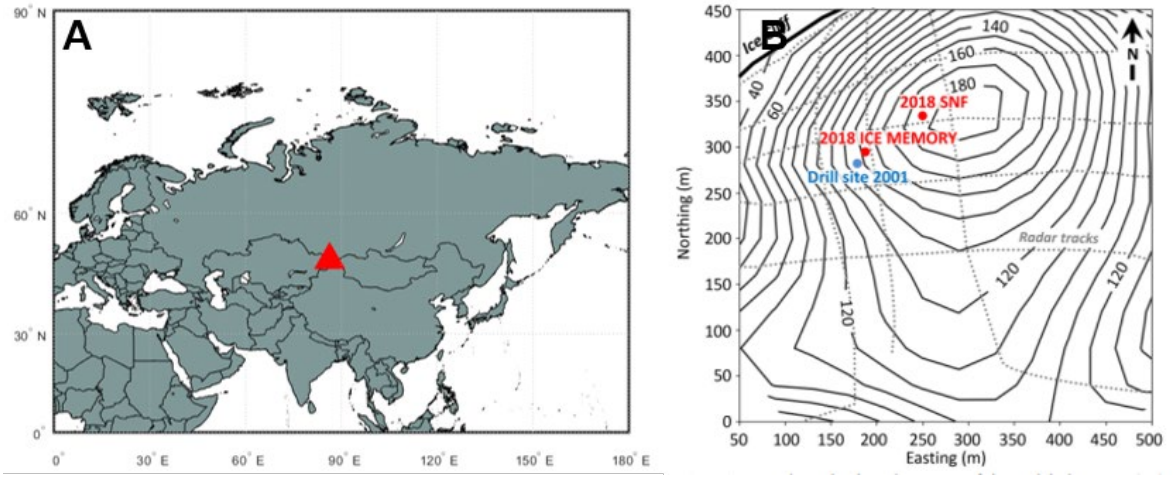

SI 2. Sample analysis.

In brief, 48.5 ± 0.9 mL (n = 65) aliquots were collected after filtering 300-500 mL of ice from a glass vessel under a helium atmosphere (Fang et al., 2019). Aliquots were spiked with 75 µL of 40 ng g^{-1} internal standard (*p*-hydroxybenzoic acid-(phenyl-$^{13}C_6$)) to achieve a final concentration of 0.055 ± 0.003 ng g^{-1} and alkalized with 8 µL of NH_4OH (25% in UPW) to pH ≈ 10. The samples were pre-concentrated using Strong Anionic Exchange (MAX, 1 mL, 10 mg bed weight, Waters) solid-phase extraction (SPE) cartridges using disposable PTFE transfer tubes at a flowrate of 1.4 ± 0.3 mL min^{-1}. The cartridges were previously conditioned with 1 mL of methanol followed by 5 mL of UPW, decontaminated using 500 µL of a 0.16 M HCl solution in methanol and exchanged in their counter ion using 500 µL of a 2% formic acid solution in UPW. After the loading step, the cartridges were wrapped in two aluminum foils and stored at -20°C for 2 months. It was previously demonstrated that this approach provides a higher analytical reproducibility compared to re-freezing the aliquots after their collection in the 50 mL glass vials (Burgay et al., 2023). Before elution, the cartridges were thawed at room temperature under a Class-1000 laminar flowhood for ≈30 min and then eluted using 3x250 µL of a 5% formic acid solution in methanol at a flowrate of 1 mL min^{-1} in pre-cleaned 1.5 mL vials. The 750-µL eluates were pre-concentrated to ≈40 µL at 30°C under a gentle N_2 flow (Reacti-Vap

Evaporator, Thermo Fischer Scientific) and then retaken with 475 µL of UPW before analysis. Subsequently, 24 ± 1 µL of 1.4 µg g^{-1} vanillin-(phenyl-$^{13}C_6$) solution (10% v/v MeOH/UPW) were added as an additional internal standard to monitor the instrument performances. The final volume was 530 ± 10 µL, indicating that the samples were enriched by a factor of 92 ± 3.

For analyses, samples were transferred to a thermostated autosampler (T = 10°C) and analyzed within 24 hours with Ultra-High Performance Liquid Chromatography (Ultimate 3000, Thermo Scientific) equipped with an Acclaim™ Organic Acid Column (3 µm, 2.1 x 150 mm, Thermo Scientific, operated at 50°C) coupled with High-Resolution Mass Spectrometry (UHPLC-HRMS, Q Exactive Focus, Thermo Scientific). The injection volume was 20 µL. Chromatographic separation was obtained using a mobile phase consisting of 0.01% formic acid, 1% acetonitrile and 1% methanol in water (v/v/v, eluent A) and methanol (eluent B) with a flow rate of 0.2 mL min^{-1}, with the following binary elution program: 0-12 min linearly increasing gradient from 8% to 90% of B, 12-15 min isocratic elution at 90% B. The ionization of compounds was performed using a heated electrospray ionization (HESI) source operating in negative mode. Data acquisition was performed in Full-MS mode with a scan range from 70 to 1000 mass-to-charge ratio (*m/z*). Instrumental conditions for electrospray ionization were: sheath gas (N_2) 35 a.u., auxiliary gas (N_2) 10 a.u., probe heater temperature 300°C, capillary temperature 280 °C and capillary voltage 2.5 kV. The MS-data were recorded in centroid mode with lock mass at *m/z* 112.98563 (sodium formate cluster). Resolution at *m/z* = 200 was 7E4. Data-dependent MS-MS (dd-MS^2) experiments were also performed with higher-energy collision dissociation (HCD) at 10, 20 and 40 au.

The analysis of the samples was performed over three months (July-September 2022). Method performances were evaluated in terms of mass accuracies, reproducibility of the retention times and internal standard intensities of $^{13}C_6$-p-hydroxybenzoic acid (^{13}C-PHBA), $^{13}C_6$-vanillin (^{13}C-VAN), succinic acid ($C_4H_6O_4$) and pinic acid ($C_9H_{14}O_4$). Mass accuracies ranged between ± 3 ppm, while the variability of the retention times was lower than 0.05 min over the entire analysis period for all the selected compounds. ^{13}C-VAN and ^{13}C-PHBA intensities were used to evaluate the instrumental sensitivity and the solid phase extraction performance, respectively. The observed variability in ^{13}C-

VAN intensity was 17.0% RSD. To consider changes in the instrumental sensitivity, data were corrected using the intensity of ^{13}C-VAN. The observed variability in ^{13}C-PHBA intensity was 17.8 RSD% (after correction), indicating an overall good reproducibility of the extractions. N=14 procedural UPW blanks were also analyzed to account for any possible contamination during the sample processing procedure and were used in the NTS workflow for background subtraction.

SI 3. Volcano plot

The volcano plot is typically constructed by plotting the logarithm ($\log_2$) of the fold change (FC) on the x-axis, and the logarithm ($-\log_{10}$) of the p-value associated with a two-sample t-test on the y-axis. The t-test and the FC depend on the definition of a specific onset, which was set here to 1955 CE. In the volcano plot related to the compounds shown in this study, we highlight those having a $\log_2$ FC > 1, $\log_2$ FC < 1 (i.e., showing more than 2-fold or less than 0.5-fold the intensity in the industrial period compared to the pre-industrial period, respectively) and a $-\log_{10}$ p-value > 1.05 (i.e., p-value > 0.05). Figure S8 shows the volcano plot for the Belukha ice core.

Other figures and tables

Figure S2 - Profile of the sum of the molecule unfiltered and uncorrected intensities (black line - 4092 molecules) and profile of the sum of the molecule filtered intensities (orange line – 491 molecules). The similar trends, corroborated by a strong correlation between the datasets (r = 0.961, p-value < 0.01) indicate that our subset is representative of the unfiltered dataset.

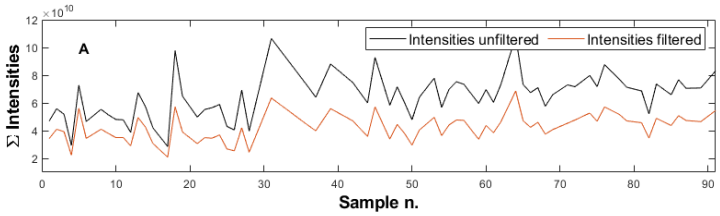

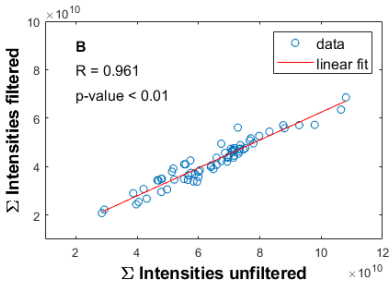

Figure S3 – Distribution of average carbon oxidation state, O/C and H/C ratios for all the molecules detected in the Belukha ice-core record and divided by clusters (see main text for details related to the clusterization).

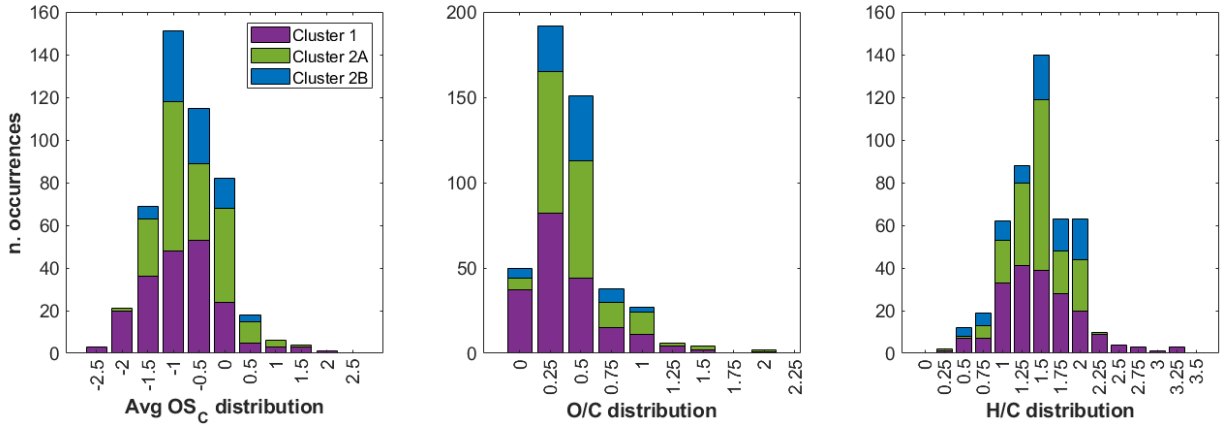

Figure S4 – Upper panel: the DBE (Double Bond Equivalent) profile shows an increase from the 1950s. Middle panels: on the left, the DBE values for industrial samples (1955-1980 CE), on the right, the DBE values for pre-industrial samples (1830-1955 CE). The color of the circles corresponds to the molecular composition of the compounds (green: CHO, violet: CHNO, red: CHOS, yellow: CHNOS, light blue: other), while the size corresponds to the average intensity calculated over the considered time period. Bottom panels: on the left, the DBE distribution for cluster 1; on the right, the DBE distribution for clusters 2A and 2B (see main text for details related to the clusterization).

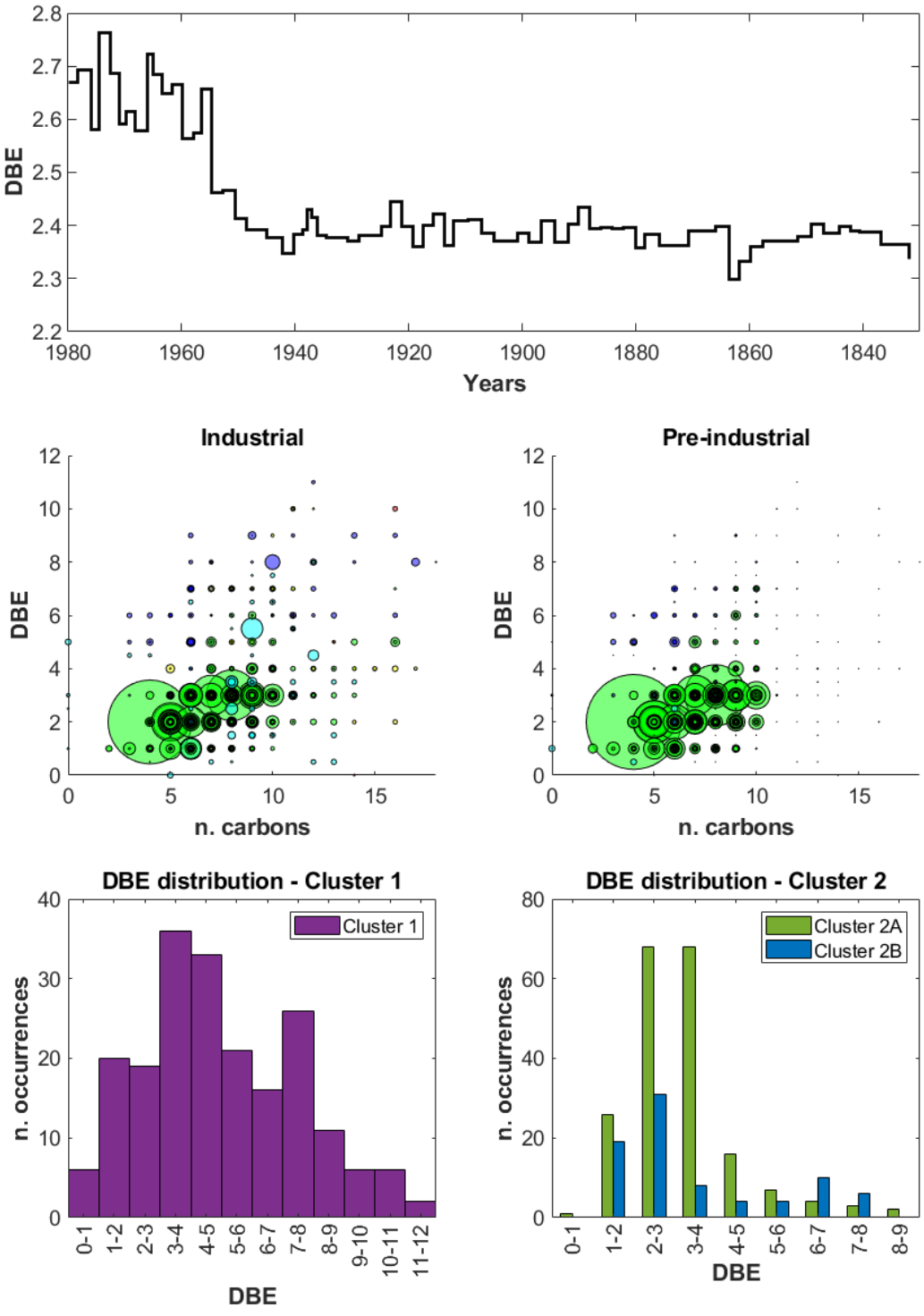

Figure S5 - Hierarchical cluster analysis of scaled data. X-axis and y-axis represent the samples and the compounds, respectively. Two clusters (1 and 2) were identified, together with two sub-clusters (2A and 2B), based on their similarities. Violet clusters are related to anthropogenic samples/compounds, green clusters refer to background samples/natural compounds.

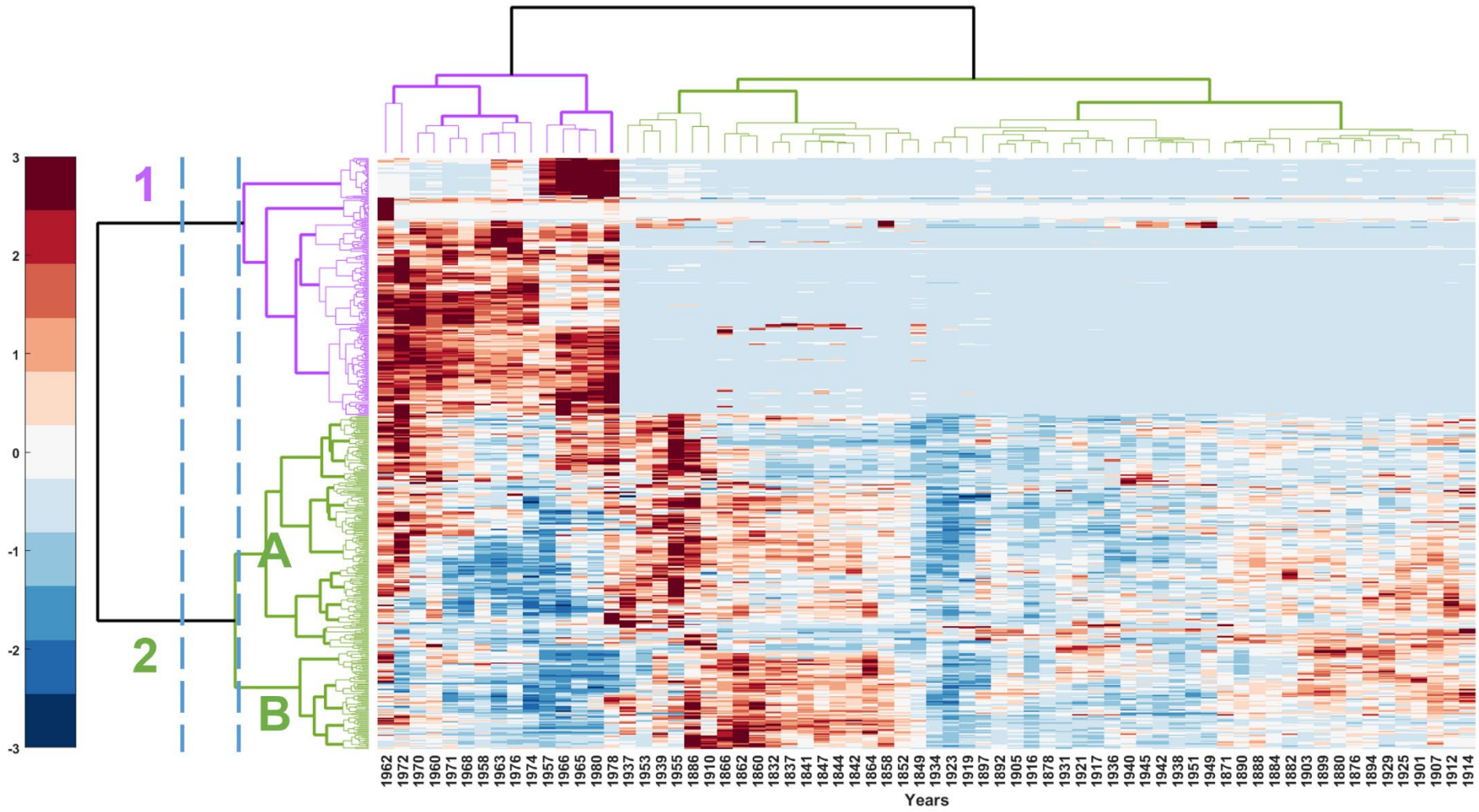

Figure S6 – 214 molecules were identified in cluster 1. The tick red line represents the ensemble mean.

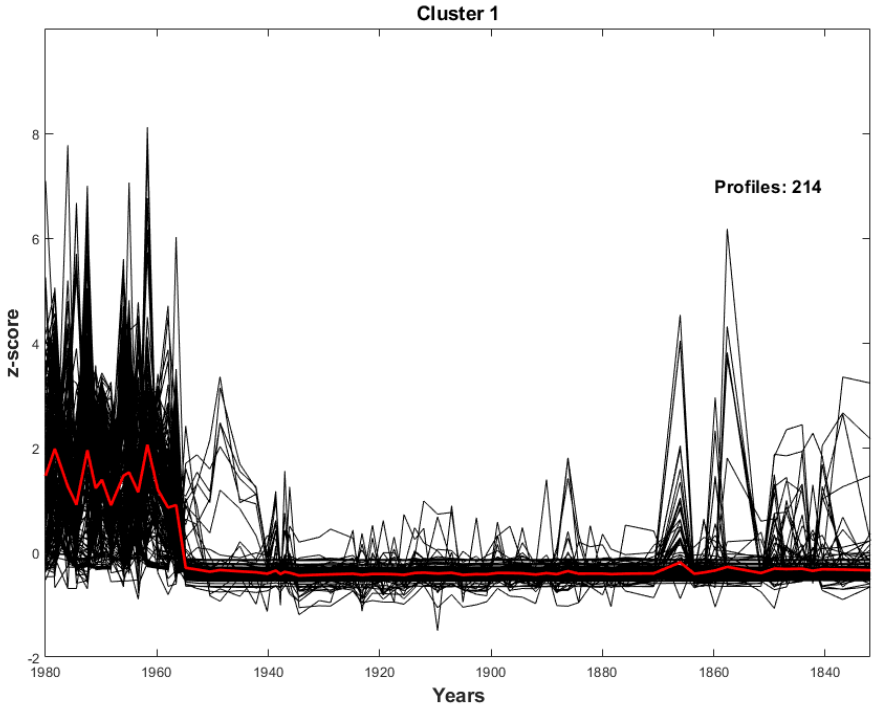

Figure S7 – 277 molecules were identified in cluster 2 (top panel), which were divided in four sub-clusters whose profiles are shown in the bottom panels. The tick red line represents the ensemble mean.

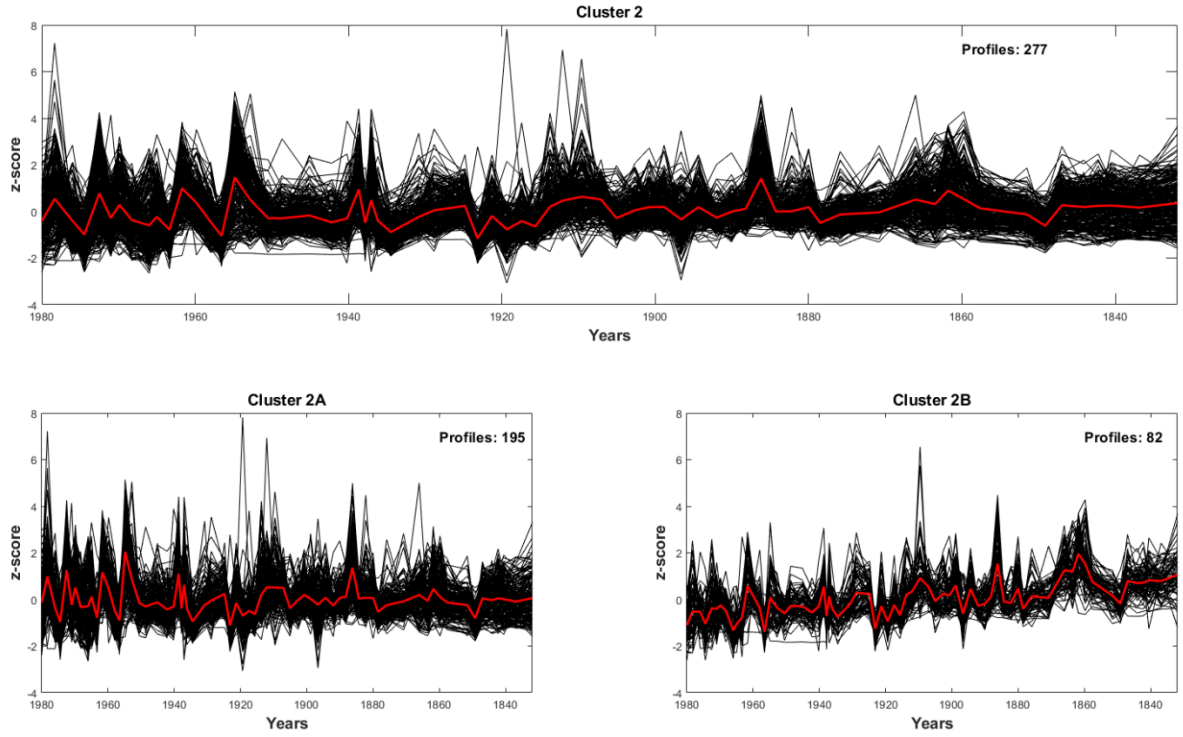

Figure S8 – The volcano plot shows which molecules occurred more (or less) in the industrial period compared to the pre-industrial period. The set thresholds are $\log_2$ Fold Change > 1, $\log_2$ Fold Change < 1 and p-value > 0.05.

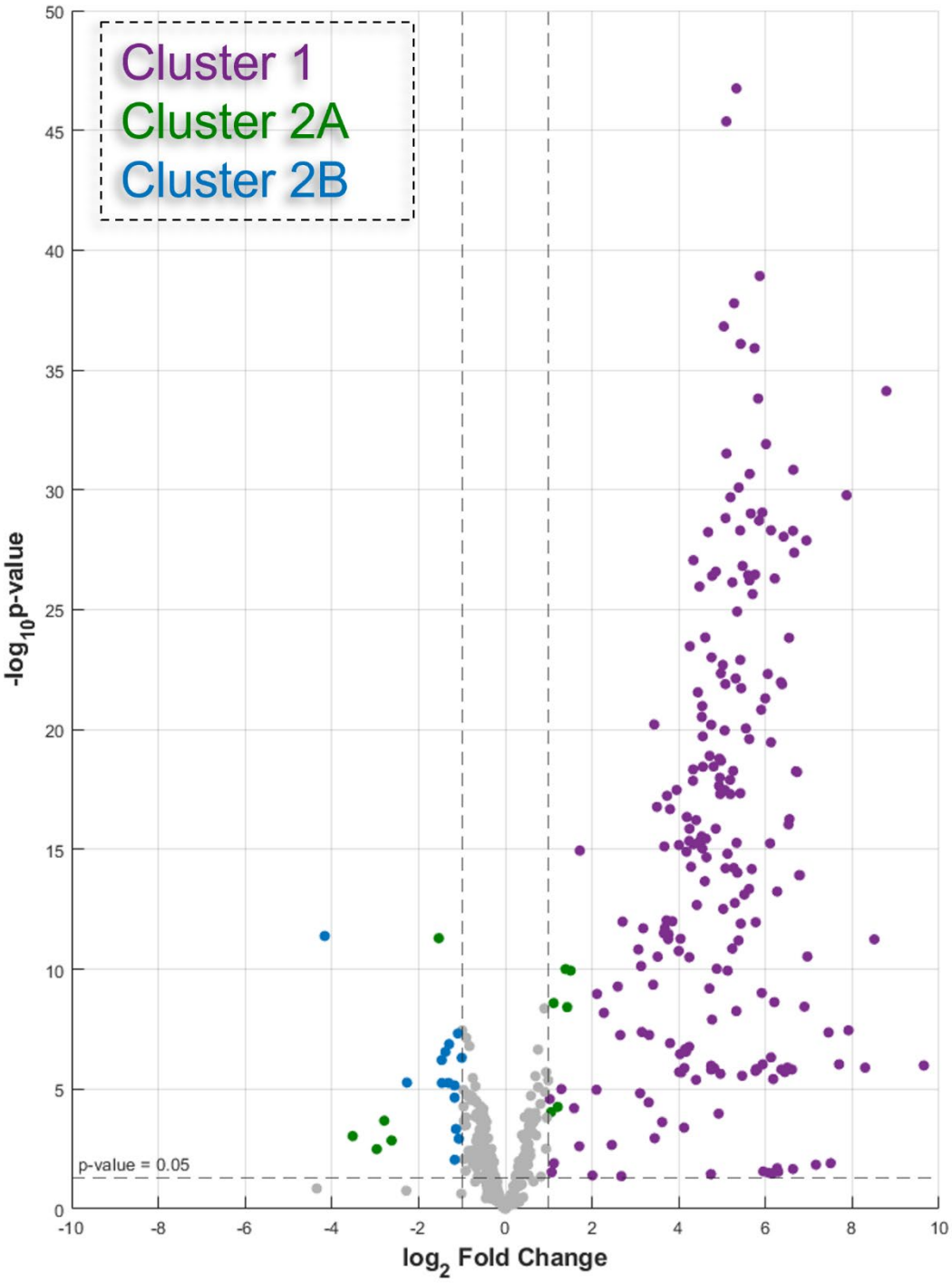

Figure S9 – Molecular characterization of the different sub-clusters. The size of the circle is scaled differently within each cluster to provide a clear visualization of all the compounds. The adoption of a unique scaling factor would have resulted into an unclear representation of the different compounds. For this reason, the circle size of this figure cannot be directly compared with the circle sizes reported in all the other figures.

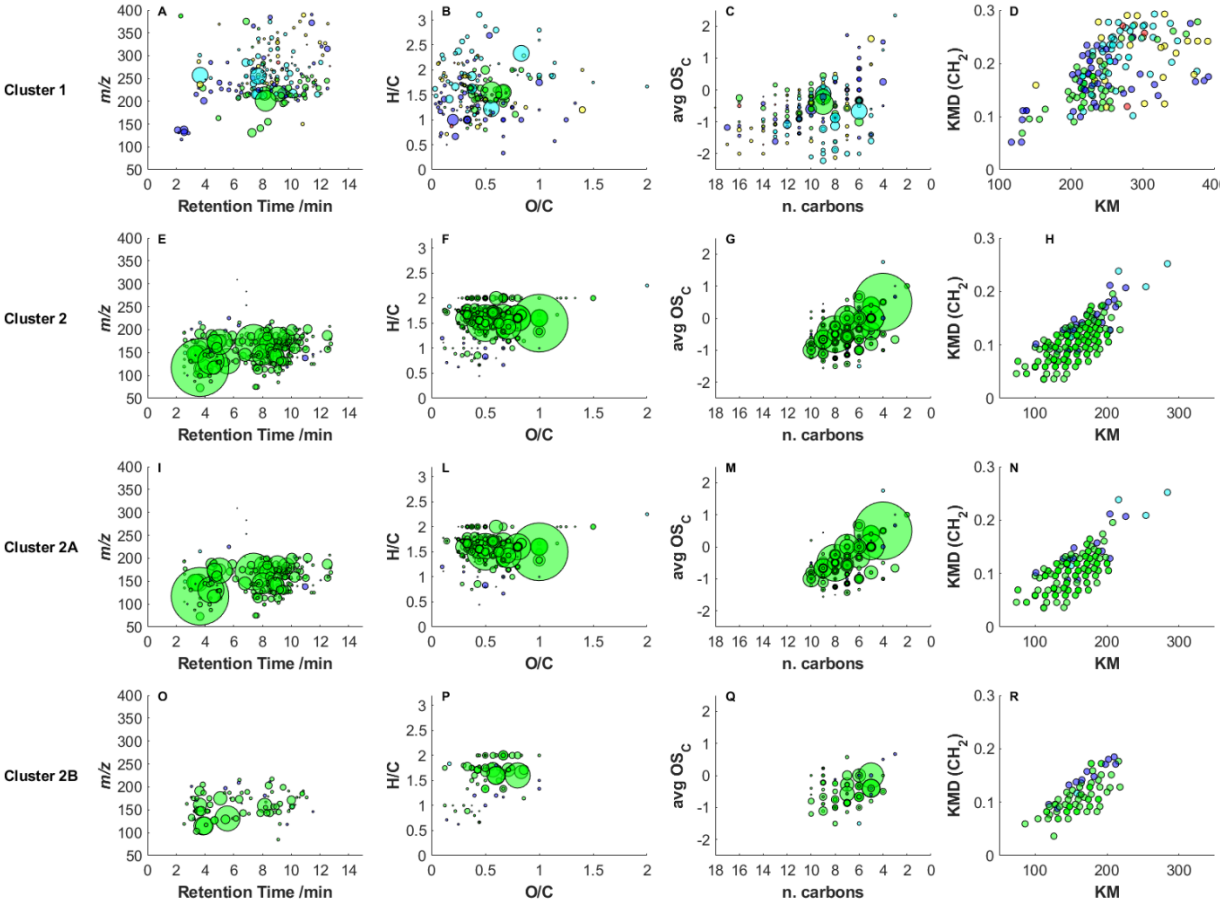

Figure S10 – Oxygen distribution showing differences between cluster 1 (red) and cluster 2 (green). The relative intensity is calculated over the total intensity for the two clusters individually.

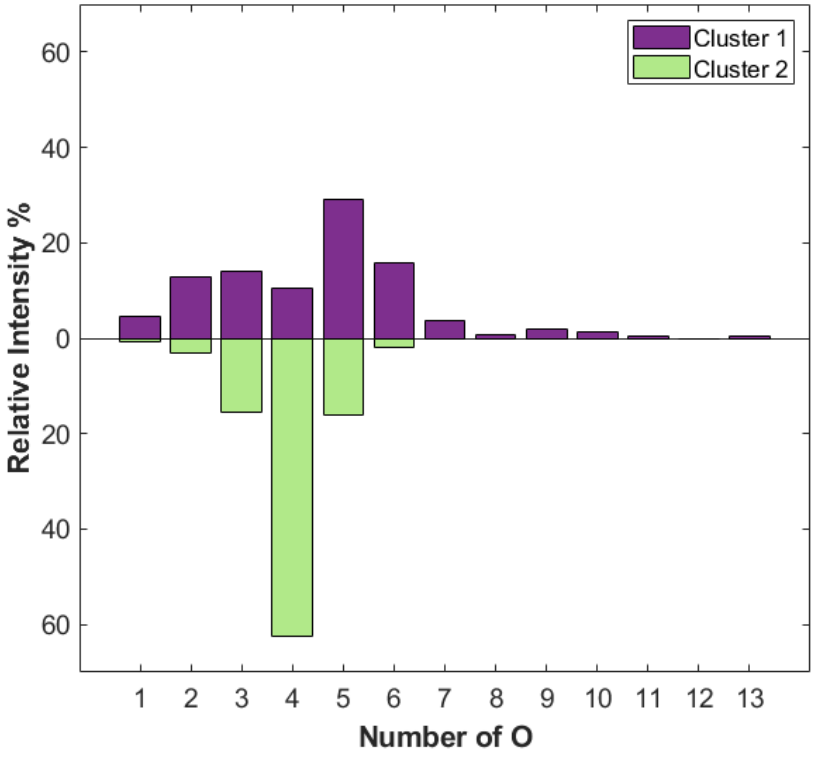

Figure S11 – Oxygen distribution within Cluster 2, divided by the two subclusters identified by performing HCA.

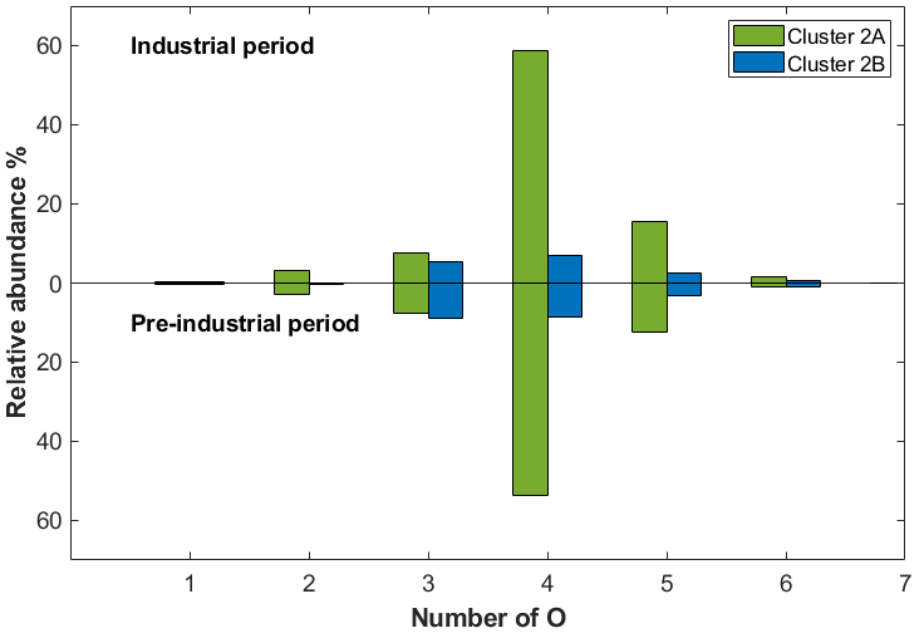

Figure S12 – Top panel: profiles of $C_7H_{10}O_5$ and $C_5H_8O_4$, as molecules representative for cluster 2A that increased during the industrial period, together with nitrate and sulphate (bottom panels).

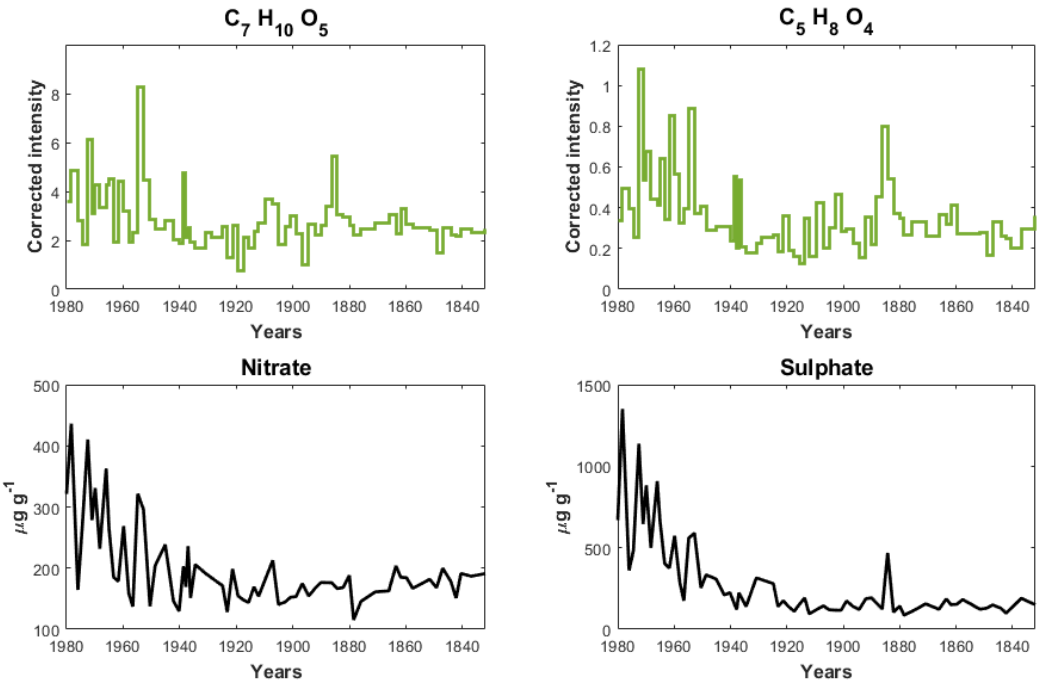

Figure S13 – Top panel: profiles of p-hydroxybenzoic acid (PHBA) and succinic acid. Bottom panel: profiles of potassium and black carbon. The multiproxy comparison between PHBA, potassium and black carbon indicates a decreasing trend of wildfires in the pre-industrial period, which is mirrored by a decreasing trend in SOA tracers, such as succinic acid, and other compounds belonging to cluster 2A.

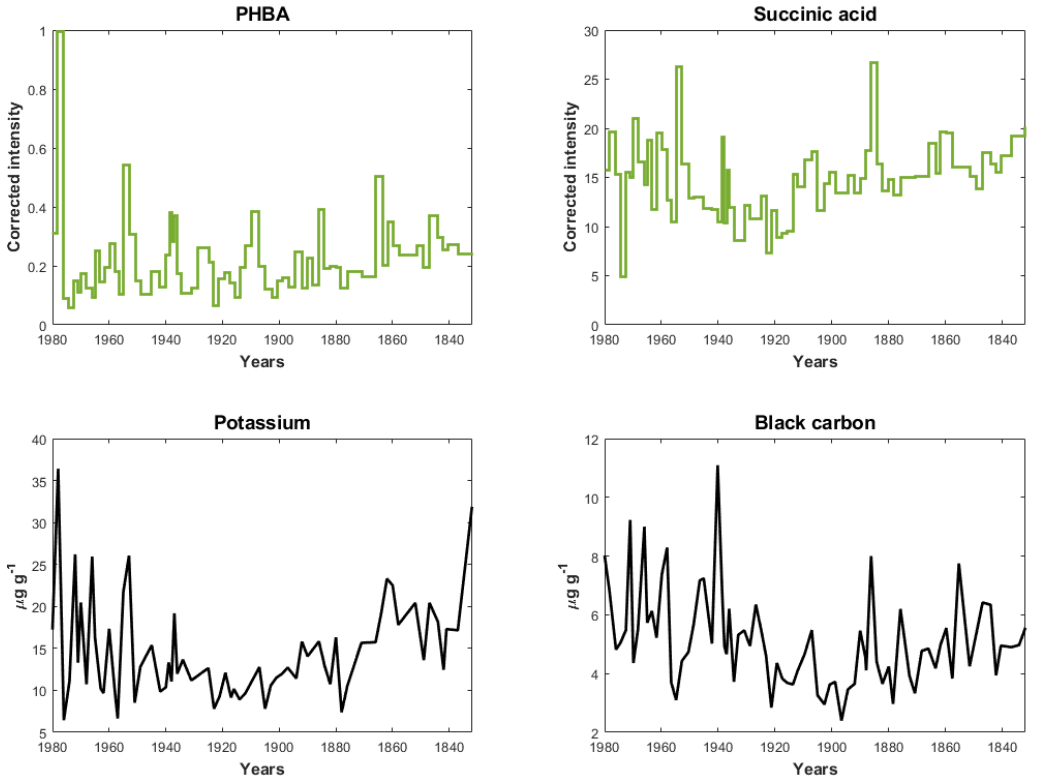

Figure S14 – Intensities of clusters 2A and 2B over time. In the industrial period is recognizable a decreasing contribution for cluster 2B in the overall intensity of cluster 2, likely due to progressively more oxidizing conditions (see main text).

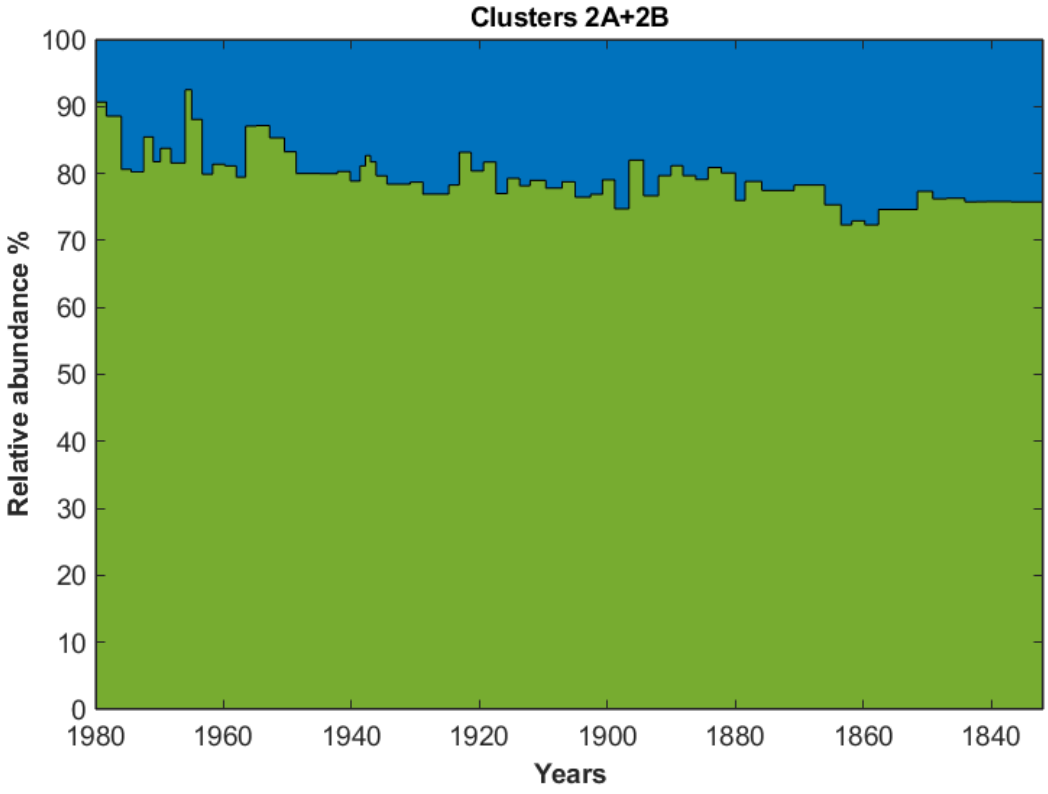

Table S1 – Years of abrupt change for Cluster 1, heavy metals, sulphate and nitrate. Pearson correlation coefficient with Cluster 1 is also reported (* indicates p-value < 0.01). Cu, Zn, Cd and Sn profiles are from Eichler et al., 2014. Pb profiles are from Eichler et al., 2012.

Element	Source	Year of abrupt change	R
Cluster 1	*Atmospheric processing or direct emissions*	1955	1
Cu	copper-nickel production (mining, smelting complexes)	1955	**0.831***
Zn	Pb-Zn, steel-Fe production	1954	**0.852***
Cd	Secondary emission from Pb-Zn and Cu-Ni production	1953	**0.633***
Sb	Secondary emission during Cu-Ni and steel-Fe production	1952	**0.777***
Pb	road traffic	1953	**0.862***
SO_4^{2-}	fossil fuel combustion	1963	**0.537***
NO_3^-	fossil fuel combustion/road traffic	1963	**0.521***

Table S2 – Identified compounds at Level 1 (n = 8), Level 2 (n = 17) and Level 3 (n = 3) using *mzCloud* as MS^2 spectral library. Only compounds with mzCloud Match ≥80 are reported.

Suspect name	**Formula**	**RT /min**	**Cluster**	**Identification Level**	**mzCloud Match**
Pimelic acid	$C_7H_{12}O_4$	8.17	2A	1	-
Sebacic acid	$C_{10}H_{18}O_4$	11.13	2A	1	-
Glutaric acid	$C_5H_8O_4$	4.44	2A	1	-
Adipic acid	$C_6H_{10}O_4$	6.41	2A	1	-
Succinic acid	$C_4H_6O_4$	3.68	2A	1	-
Levulinic acid	$C_5H_8O_3$	3.87	2B	1	-
Pinic acid	$C_9H_{14}O_4$	9.03	2A	1	-
p-hydroxybenzoic acid	$C_7H_6O_3$	8.55	2A	1	-
3-Methylsalicylic acid	$C_8H_8O_3$	9.83	2B	2	97.6
3,3 Dimethylglutaric acid	$C_7H_{12}O_4$	8.54	2A	2	95.9
4-hydroxy-2-methylbenzoic acid	$C_8H_8O_3$	9.83	2B	2	94.2
Glycolic acid	$C_2H_4O_3$	7.52	2A	2	92.9
4-hydroxyphenylacetic acid	$C_8H_8O_3$	9.83	2B	2	92.9

2,3-dihydroxypropanoic acid	$C_3H_6O_4$	2.57	2A	2	92.9
p-nitrophenol	$C_6H_5NO_3$	10.94	2A	2	92.7
Isobutyric acid	$C_4H_8O_2$	4.41	2A	2	91.5
3-methyladipic acid	$C_7H_{12}O_4$	8.54	2A	2	91.2
4-hydroxybenzaldehyde	$C_7H_6O_2$	8.88	2A	2	86.9
Ciclohexanecarbozylic acid	$C_7H_{12}O_2$	7.91	2A	2	86.3
Camphanic acid	$C_{10}H_{14}O_4$	8.57	2A	2	85.7
Caffeic acid	$C_9H_8O_4$	8.37	2B	2	85.4
p-hydroxymethyl-benzoic acid	$C_8H_8O_3$	9.83	2B	2	85.2
N-Isobutyrylglicine	$C_6H_{11}NO_3$	7.72	2A	2	84.3
2-hydroxycinnamic acid	$C_9H_8O_3$	9.20	2B	2	83.5
2-hydroxyphenylacetic acid	$C_8H_8O_3$	9.83	2B	2	82.5
4-hydroxyphenylpyruvic acid	$C_9H_8O_4$	8.37	2B	2	81.8
2,3-dihydro-1,4-benzodioxine-5-carboxylic acid	$C_9H_8O_4$	8.37	2B	2	81.5
Cyclopentylacetic acid	$C_7H_{12}O_2$	7.91	2A	2	80.8

References

Burgay, F., Salionov, D., Huber, C. J., Singer, T., Eichler, A., Ungeheuer, F., Vogel, A., Schwikowski, M., and Bjelić, S. a.: Hybrid Targeted/Untargeted Screening Method for the Determination of Wildfire and Water-Soluble Organic Tracers in Ice Cores and Snow, Analytical chemistry, 2023.

Fang, L., Schindler, J., Jenk, T., Uglietti, C., Szidat, S., and Schwikowski, M.: Extraction of dissolved organic carbon from glacier ice for radiocarbon analysis, Radiocarbon, 61, 681-694, 2019.